

**CLASSIFICATION OF DEFECT TYPES IN XLPE CABLE
JOINTS USING PARTIAL DISCHARGE MEASUREMENT**

NURLIANA BINTI ABU BAKAR

**FACULTY OF ENGINEERING
UNIVERSITY OF MALAYA
KUALA LUMPUR**

2018

**CLASSIFICATION OF DEFECT TYPES IN XLPE CABLE
JOINTS USING PARTIAL DISCHARGE MEASUREMENT**

NURLIANA BINTI ABU BAKAR

**DISSERTATION SUBMITTED IN FULFILMENT OF
THE REQUIREMENTS FOR THE DEGREE OF MASTER
OF ENGINEERING**

**FACULTY OF ENGINEERING
UNIVERSITY OF MALAYA
KUALA LUMPUR**

2018

UNIVERSITY OF MALAYA
ORIGINAL LITERARY WORK DECLARATION

Name of Candidate: **Nurliana Binti Abu Bakar**

I.C/Passport No:

Matric No: **KQI160001**

Name of Degree: **Master of Engineering**

Title of Research Report: **Classification of Defect Types in XLPE Cable Joints
Using Partial Discharge Measurement**

Field of Study: **High Voltage Engineering**

I do solemnly and sincerely declare that:

- (1) I am the sole author/writer of this Work;
- (2) This Work is original;
- (3) Any use of any work in which copyright exists was done by way of fair dealing and for permitted purposes and any excerpt or extract from, or reference to or reproduction of any copyright work has been disclosed expressly and sufficiently and the title of the Work and its authorship have been acknowledged in this Work;
- (4) I do not have any actual knowledge nor do I ought reasonably to know that the making of this work constitutes an infringement of any copyright work;
- (5) I hereby assign all and every rights in the copyright to this Work to the University of Malaya ("UM"), who henceforth shall be owner of the copyright in this Work and that any reproduction or use in any form or by any means whatsoever is prohibited without the written consent of UM having been first had and obtained;
- (6) I am fully aware that if in the course of making this Work I have infringed any copyright whether intentionally or otherwise, I may be subject to legal action or any other action as may be determined by UM.

Candidate's Signature

Date:

Subscribed and solemnly declared before,

Witness's Signature

Date:

Name:

Designation:

ABSTRACT

Cross-linked polyethylene (XLPE) cables are broadly used in power industries due to their excellent mechanical and electrical properties. Cable joints are the weakest part in XLPE cables and prone to failures of the insulation. Breakdown in cable joint insulation can cause large losses to the power companies. Therefore, it is important to analyse the quality of insulation for the early detection of insulation failure. It is known that there is a relationship between partial discharge (PD) and the quality of the insulation. PD is one of the important phenomena that engineers should take care of in high voltage (HV) engineering. PD analysis is an important tool for evaluating the quality of insulation in cable joints. In this work, three XLPE cable joints with artificial created defects, which are commonly found on site, have been prepared. The input data from PD measurement results were used to train the artificial intelligence methods to classify each type of defect in the samples of cable joints. The feature extractions composed of statistical features and principle components analysis (PCA) after discrete Fourier transform (DFT), discrete wavelet transform (DWT) and wavelet packet transform (WPT) were applied on PD signals. Classifications were implemented using two different types of classifiers, support vector machine (SVM) and artificial neural network (ANN). The performance of each feature extraction method and classifier were evaluated. The proposed methods were compared with the existing methods to confirm the advantages of the proposed methods over the available methods. From the comparison of the results obtained, it was found that statistical features with DFT signals classified by ANN yield the highest accuracy among all of the methods tested.

ABSTRAK

Kabel polietilena bersilang (XPLE) digunakan secara meluas dalam industri kuasa kerana sifat-sifat mekanikal dan elektrikalnya yang sangat baik. Sambungan kabel adalah bahagian yang paling lemah dalam kabel XLPE dan terdedah kepada kegagalan penebat. Kerosakan pada sambungan kabel penebat boleh menyebabkan kerugian besar kepada syarikat-syarikat kuasa. Oleh itu, adalah penting untuk menganalisis kualiti penebat untuk pengesanan awal kegagalan penebat. Adalah diketahui bahawa terdapat hubungan antara pelepasan separa (PD) dan kualiti penebat. PD adalah salah satu fenomena penting yang harus dijaga oleh jurutera dalam kejuruteraan voltan tinggi (HV). Analisis PD adalah alat penting untuk menilai kualiti penebat dalam sambungan kabel. Dalam kerja ini, tiga sambungan kabel XLPE dengan kecacatan buatan dibuat, yang biasanya yerdapat di tapak, telah disediakan. Data input dari hasil pengukuran PD digunakan untuk melatih kaedah kecerdasan buatan untuk mengklasifikasikan setiap jenis kecacatan dalam sampel sambungan kabel. Pengekstrakan ciri yang terdiri daripada ciri-ciri statistik dan analisis komponen asas (PCA) selepas transformasi Fourier diskret (DFT), transformasi wavelet diskret (DWT) dan transformasi paket wavelet (WPT) telah digunakan pada isyarat PD. Pengelasan telah dilaksanakan menggunakan dua jenis pengelas, mesin vektor sokongan (SVM) dan rangkaian saraf buatan (ANN). Prestasi setiap kaedah ciri pengekstrakan dan pengelas dinilai. Kaedah yang dicadangkan telah dibandingkan dengan kaedah sedia ada untuk mengesahkan kelebihan kaedah yang dicadangkan melalui kaedah yang ada. Daripada perbandingan hasil yang diperolehi, didapati bahawa ciri-ciri statistik dengan isyarat DFT dikelaskan oleh ANN menghasilkan ketepatan tertinggi di antara semua kaedah yang diuji.

ACKNOWLEDGEMENTS

My upmost gratitude goes to God, the most gracious, most merciful, for His blessings, which giving me strength and a good health in completing this project. I would like to give my deepest appreciation to my supervisor, Associate Professor Ir. Dr. Hazlee Azil Bin Illias for his continuous support, time and discussion during the development of this research. His willingness to assist, give guidance, suggestions and ideas has made me able to complete this project. Last but not least, thanks to my families for all their endless prayers, supports, which have provided me strength and courage to complete this project. Not forgetting, I would like to express my appreciation to all lecturers that giving me all the basic needed for completing this project.

University of Malaya

TABLE OF CONTENTS

ABSTRACT	iii
ABSTRAK	iv
ACKNOWLEDGEMENTS	v
TABLE OF CONTENTS	vi
LIST OF FIGURES	ix
LIST OF TABLES	xi
LIST OF ABBREVIATIONS	xiii
CHAPTER 1: INTRODUCTION	1
1.1 Background.....	1
1.2 Problem Statement.....	3
1.3 Objectives of Research	3
1.4 Dissertation Structure	4
CHAPTER 2: PARTIAL DISCHARGE PHENOMENON	5
2.1 Introduction	5
2.2 Introduction of Partial Discharge	5
2.3 Types of Partial Discharge	7
2.3.1 Internal Discharge	7
2.3.2 Corona Discharge	8
2.3.3 Surface Discharge.....	9
2.4 Partial Discharge Measurement Methods.....	9
2.4.1 Optical Measurement Method	10
2.4.2 Acoustic Measurement Method.....	12
2.4.3 Chemical Measurement Method	13

2.4.4	Electrical Measurement Method	14
2.5	Previous Partial Discharge Classification Works	16
2.5.1	Partial Discharge Classification using Support Vector Machine	16
2.5.2	Partial Discharge Classification using Artificial Neural Network	18
CHAPTER 3: PARTIAL DISCHARGE MEASUREMENT.....		23
3.1	Introduction	23
3.2	Project Development	23
3.3	Cable Joint Samples Preparation	24
3.4	Partial Discharge Measurement Setup.....	26
3.5	Partial Discharge Feature Extractions	28
3.5.1	Statistical Features.....	29
3.5.2	Principle Component Analysis.....	32
3.6	Partial Discharge Signal Processing Techniques.....	33
3.6.1	Discrete Fourier Transform.....	33
3.6.2	Discrete Wavelet Transform	34
3.6.3	Wavelet Packet Transform	37
3.7	Partial Discharge Classifiers	38
3.7.1	Support Vector Machine	38
3.7.2	Artificial Neural Network	39
CHAPTER 4: RESULTS AND DISCUSSIONS.....		42
4.1	Introduction	42
4.2	Classification Results by Support Vector Machine.....	42
4.2.1	Statistical Features with Discrete Fourier Transform.....	43
4.2.2	Statistical Features with Discrete Wavelet Transform	47
4.2.3	Statistical Features with Wavelet Packet Transform.....	52

4.3	Classification Results by Artificial Neural Network	57
4.3.1	Statistical Features with Discrete Fourier Transform.....	58
4.3.2	Statistical Features with Discrete Wavelet Transform	63
4.3.3	Statistical Features with Wavelet Packet Transform.....	67
4.3.4	PCA Feature with Discrete Fourier Transform	73
4.3.5	PCA Feature with Discrete Wavelet Transform.....	74
4.3.6	PCA Feature with Wavelet Packet Transform	75
4.4	Overall Best Results of SVM and ANN Classification	77
4.4.1	Statistical Features of SVM and ANN Classifiers	77
4.4.2	PCA Feature of ANN Classifier	79
4.5	Comparison with Previous Works	80
 CHAPTER 5: CONCLUSIONS AND RECOMMENDATIONS.....		82
5.1	Conclusions	82
5.2	Recommendations for Future Works.....	82
 REFERENCES.....		83

LIST OF FIGURES

Figure 2.1: Power cable defects	6
Figure 2.2: Percentages of cables subjected to PD	6
Figure 2.3: Internal discharge	8
Figure 2.4: Corona discharge	9
Figure 2.5: Surface discharge.....	9
Figure 2.6: Experimental test setup; (1) Optical sensor, (2) Optical fibre, (3) Coupling capacitor, (4) HV supply, (5) Voltage divider, (6) Peak plate, (7) Oil container	11
Figure 2.7: Theory of the optical PD measurement.....	11
Figure 2.8: Acoustic sensor; a) Sensor of piezoelectric film with connector, (b) Standard scheme of the piezoelectric transducer sensor	12
Figure 2.9: Hydrogen oil detector	14
Figure 2.10: Direct probing method.....	15
Figure 3.1: Flowchart of the project.....	24
Figure 3.2: Defects created; (a) Insulation incision defect, (b) Axial direction shift defect, (c) Semiconductor layer tip defect	25
Figure 3.3: Configuration of PD measurement under AC voltage.....	26
Figure 3.4: PD measurement setup in HV laboratory	27
Figure 3.5: Power bench in HV laboratory	28
Figure 3.6 (a): Positively skewed distribution	30
Figure 3.6 (b): Symmetrical distribution.....	30
Figure 3.6 (c): Negatively skewed distribution.....	30
Figure 3.7: Positive, negative and normal kurtosis	31
Figure 3.8: Sine wave signal	35

Figure 3.9: Wavelet signal	35
Figure 3.10: DWT dilation representation	36
Figure 3.11: WPT dilation representation.....	37
Figure 3.12: Optimum hyperplane diagram.....	39
Figure 3.13: Sigmoid function	40
Figure 3.14: Feed-forward network	41
Figure 4.1: SVM accuracy average reading at different SNR for DFT signal.....	47
Figure 4.2: SVM accuracy average reading at different SNR for DWT signal.....	52
Figure 4.3: SVM accuracy average reading at different SNR for WPT signal.....	57
Figure 4.4: ANN accuracy average reading at different SNR for DFT signal.....	62
Figure 4.5: ANN accuracy average reading at different SNR for DWT signal.....	67
Figure 4.6: ANN accuracy average reading at different SNR for WPT signal.....	72
Figure 4.7: ANN accuracy average reading at different SNR for PCA feature.....	77
Figure 4.8: Overall accuracy at different signal for statistical features	78
Figure 4.9: Overall accuracy at different signal for PCA feature	79

LIST OF TABLES

Table 3.1: Samples of XLPE cable joints defects	25
Table 4.1: SVM accuracy for DFT-mean	43
Table 4.2: SVM accuracy for DFT-standard deviation.....	44
Table 4.3: SVM accuracy for DFT-kurtosis	45
Table 4.4: SVM accuracy for DFT-skewness	46
Table 4.5: SVM accuracy average reading for DFT signal	47
Table 4.6: SVM accuracy for DWT-mean.....	48
Table 4.7: SVM accuracy for DWT-standard deviation	49
Table 4.8: SVM accuracy for DWT-kurtosis.....	50
Table 4.9: SVM accuracy for DWT-skewness	51
Table 4.10: SVM accuracy average reading for DWT signal.....	52
Table 4.11: SVM accuracy for WPT-mean.....	53
Table 4.12: SVM accuracy for WPT-standard deviation.....	54
Table 4.13: SVM accuracy for WPT-kurtosis.....	55
Table 4.14: SVM accuracy for WPT-skewness	56
Table 4.15: SVM accuracy average reading for WPT signal.....	57
Table 4.16: ANN accuracy for DFT-mean	58
Table 4.17: ANN accuracy for DFT-standard deviation.....	59
Table 4.18: ANN accuracy for DFT-kurtosis	60
Table 4.19: ANN accuracy for DFT-skewness	61
Table 4.20: ANN accuracy average reading for DFT signal.....	63
Table 4.21: ANN accuracy for DWT-mean.....	63

Table 4.22: ANN accuracy for DWT-standard deviation	64
Table 4.23: ANN accuracy for DWT-kurtosis.....	65
Table 4.24: ANN accuracy for DWT-skewness	66
Table 4.25: ANN accuracy average reading for DWT signal.....	67
Table 4.26: ANN accuracy for WPT-mean.....	68
Table 4.27: ANN accuracy for WPT-standard deviation.....	69
Table 4.28: ANN accuracy for WPT-kurtosis.....	70
Table 4.29: ANN accuracy for WPT-skewness	71
Table 4.30: ANN accuracy average reading for WPT signal.....	72
Table 4.31: ANN accuracy for DFT-PCA	73
Table 4.32: ANN accuracy for DWT-PCA.....	74
Table 4.33: ANN accuracy for WPT-PCA	75
Table 4.34: ANN accuracy average reading for PCA feature.....	76
Table 4.35: Best results of statistical features.....	78
Table 4.36: Best results of PCA feature.....	79
Table 4.37: Comparison with the past works.....	80

LIST OF ABBREVIATIONS

AC	: Alternating current
ANN	: Artificial neural network
BPNN	: Back-propagation neural network
DC	: Direct current
DFT	: Discrete Fourier transform
DGA	: Dissolve gas analysis
DWT	: Discrete wavelet transform
EMI	: Electromagnetic interference
ENN	: Ensemble neural network
FFT	: Fast Fourier transform
GIS	: Gas insulated switchgear
HPLC	: High performance liquid chromatography
HV	: High voltage
IEC	: International electro-technical commission
MNN	: Modular neural network
pC	: pico-Coulombs
PC	: Personal computer
PCA	: Principle component analysis
PD	: Partial discharge
PET	: Polyethylene terephthalate
PILC	: Paper insulated lead covered
PNN	: Probabilistic neural network
PRPD	: Phase resolved partial discharge
RBPNN	: Radial basis probabilistic neural network
RHPNN	: Robust heteroscedastic probabilistic neural network
SF ₆	: Sulphur hexafluoride
SNN	: Single neural network
SNR	: Signal-to-noise-ratio
SVM	: Support vector machine
TRPD	: Time resolved partial discharge
WPT	: Wavelet packet transform
XLPE	: Cross-linked polyethylene

CHAPTER 1: INTRODUCTION

1.1 Background

Life span operation of the important power system equipment, for example high voltage (HV) cables, transformers and gas insulated switchgear (GIS) are highly dependent on the quality of the insulation. Power system equipment will be permanently impaired in the event of insulation breakdown. Any part in the power equipment that has failure will affect transmission and power generation businesses. Therefore, it is vital to examine and observe the insulation quality of power system equipment regularly. According to failure analysis, damage for more than half of HV equipment is due to insulation failure (Tian, Lewin et al. 2002). Cross-linked polyethylene (XLPE) has balanced electrical, mechanical and thermal materials (Chen, Xu et al. 2014) and has been widely used for HV cables insulation (Cho, Shim et al. 1998). Cable joints in the XLPE are the weakest part by the reason of insulation discontinuity and human nature of its creation (Hunter, Lewin et al. 2013).

Insulation performance is much influenced by the activities of partial discharge (PD). Partial Discharge (PD) is defined by IEC 60270 (Partial Discharge Measurements) as a localized electrical discharge that partially bridges the insulation between conductors and which may or may not occur adjacent to a conductor (Standard 2000). PD is recurring in nature (Mota, Rocha et al. 2011) (Illias, Yuan et al. 2012) and is able to propagate across the dielectric material. This can cause serious destruction to the insulation and decrease the life span of HV equipment (Angrisani, Daponte et al. 2000). Continuous PD also degrades insulation materials, which finally results in damage of insulation and disturb the consistency of the power system (Mardiana and Su 2010) (Zhang, Xiao et al. 2014). PD enhances the existing insulation deterioration and causes fixed deterioration of the insulating quality, in the end leading to electrical damage,

danger to personnel, damage to the environment and the failure of expensive equipment (Song, Zhou et al. 2007).

Different defects, for example voids and impurities in power cables insulation may appear throughout the industrial process and can be a major PD source activities (Lei, Song et al. 2014) (Tian, Lewin et al. 2002). PD can be divided into three types, internal discharge develops in cavities or voids within liquid or solid dielectric, surface discharge presents at the edge of insulation material and corona discharge appears in gaseous dielectric in the existence of inhomogeneous field (Kuffel and Kuffel 2000). PD that occurs at the defect site will cause the production of sound, heat, light or a chemical reaction (Lu, Su et al. 2018). Since PD events can affect the safety and finance, tracking the occurrence of PD is used as the main method in monitoring the state of the insulation system (de Oliveira Mota, da Rocha et al. 2011).

Detection and identifying of PD activity is important at the beginning so that replacement is scheduled at the appropriate time (Ma, Zhou et al. 2002). PD classification is essential to assess the risk of insulation damage and can determine current component that needs service or replacement (Hoof, Freisleben et al. 1997). Measurement of PD is recognised as a diagnostic tool for assessing the power cables condition and can enhance the reliability of the power system by giving early attention to prevent utility interruption (Mohamed, Siew et al. 2013) (Mohamed, Siew et al. 2014). This evaluation is a typical electrical test as specified in IEC 60270 standards and is usually performed offline with a filtered laboratory to detect defects in solid insulation. Several pico-Coulombs (pC) of PD pulse magnitude can be a reason of permanent destruction to dielectric insulation. Therefore, it is important to detect PD in cables and remove their primary source to avoid failures to the whole system (Lemke 2013) (Sheng, Zhou et al. 2014). It is also vital to evaluate cable insulation as

maintenance and replacement of cable operations is needed so that unexpected failure can be avoided.

1.2 Problem Statement

Many research works have been performed on the classification of cross-linked polyethylene (XLPE) cable joints defect types and they have improved over the years. However, a perfect method has yet to be achieved. Hence, a more detailed research is needed for how different extracted partial discharge (PD) signals levels affect the classification accuracy of cable joints defect types. The most suitable method that can be used to classify XLPE cable joints defect types using PD measurement is identified in the end of this work.

In this work, classification of defect types in XLPE cable joints using PD measurement has been performed. The measurement of PD has been applied to three XLPE cable joints with a various artificial defects. Two different feature extraction methods with three signal processing techniques were applied to obtain the input from the PD data for the classification of cable joints defects. Then, the performance between different feature extractions, artificial intelligence methods and the existing works has been compared.

1.3 Objectives of Research

The objectives of this work are:

1. To perform measurement of partial discharge (PD) from artificially prepared cross-linked polyethylene (XLPE) cable joint defects
2. To apply different extraction method on partial discharge (PD) signals for classification of cable joint defects

3. To compare the performance between different feature extractions, artificial intelligence methods and the existing work

1.4 Dissertation Structure

Chapter 1 explains the background of the research, problem statement and objectives of the works. All of these topics are presented through this chapter. Chapter 2 deals with the theories about partial discharge (PD). This chapter also includes literature review from the previous research works related to PD phenomenon. In Chapter 3, the methodology of the work is presented in details to accomplish the objectives of this research. This comprises the arrangement of the cross-linked polyethylene (XLPE) cable joints, setup of the PD measurement and application of feature extraction methods and classifiers. Chapter 4 discusses all classification and measurement results that have been carried out in this work. This chapter also describes the difference between the various types of input features and classifiers and the results are also compared with the existing works. Finally, Chapter 5 is about the conclusions of the work and recommendations of upcoming works that can be implemented for this research.

CHAPTER 2: PARTIAL DISCHARGE PHENOMENON

2.1 Introduction

This chapter starts with information about partial discharge (PD) and types of PD. Methods of PD measurement are also explained because it is one of the diagnostic tools to detect defects in insulating power cables so that sudden failure of the entire power system of high voltage can be avoided. Detailed review of the previous PD classification works is also presented.

2.2 Introduction of Partial Discharge

Early diagnosis of high voltage (HV) equipment especially for the diagnosis of insulation failure is important to ensure the dependability of the entire power system (Chen, Chen et al. 2014). Partial discharge (PD) is the main reason behind the sudden failure, which damages the insulation due to charge bombardment on insulation surface, resulting in chemical and physical deterioration and can cause unexpected breakdown (Ghaffarian Niasar 2012). PD is an electrical discharge that happens in the insulation of HV equipment usually caused by the presence of cavity or pollution, resulting in the failure of the manufacturing process, mechanical pressure or aging (Mota, Rocha et al. 2011). Therefore, it is essential to observe the insulation used in the HV system to plan maintenance action at the right time.

Breakdown occurs due to damage in cable insulation. Therefore, power cables have a great significance in power system. Power cables usually include filters, conductor, semi-conductive screens, jacket, shield and insulation. There are two main categories of cables, which are cross-linked polyethylene (XLPE) insulation or impregnated paper (Su and Li 2013). The failures of the cables system or its accessories can have an effect

on the overall power system's reliability. Figure 2.1 shows an example of power cable defects (Lei, Song et al. 2014).

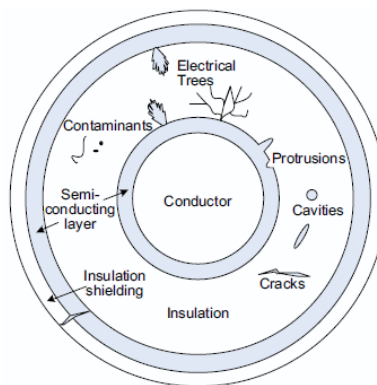


Figure 2.1: Power cable defects (Lei, Song et al. 2014)

Damage in cables of power is commonly attributed by excavate activities (Gulski, Wester et al. 2002). However, damage for more than half in the cable network is due to internal damage in the network cable insulation system. Withstand test (AC and DC) is a test method that is only used in power cables network for many years but nowadays, PD test has also become a generally accepted method. PD is one of the main sources for cable insulation deterioration in service or practice. PD degrades the insulation and may result in loss of energy. 67% of cable failure cases are located in concentrated PD, which is higher in percentage (Noske and Rakowska 2014). Figure 2.2 shows the percentages of cables that are subjected to PD activity in the failure place.

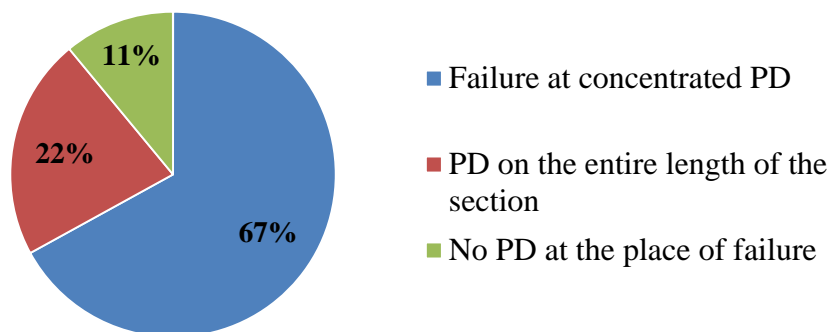


Figure 2.2: Percentages of cables subjected to PD (Noske and Rakowska 2014)

Cables and accessories include joints and terminations in the system of power cables. The function of joints is to join two cables with each other while terminations are to prepare the cable's end. PD defects usually occur in cables joints and terminations from the cable itself as they are regularly installed with imperfect conditions (Evagorou, Kyprianou et al. 2010). The XLPE cable joint failure rate is higher than the cable in the distribution system due to poor environmental conditions, incorrect installation and aging (Hui, Liu et al. 2016). In order to prevent deterioration of insulation, there are many factors to be considered during the installation of cables accessories. Skilled professional of cables jointers are required in installation of cable joints as it is a very delicate job.

2.3 Types of Partial Discharge

The insulation materials of equipment take different form of solid, liquid and gaseous and it is known that there is no perfect insulation in high voltage (HV) system. Therefore, the presence of impurities or bubbles will give the partial discharge (PD) opportunity to occur and affect the quality of insulation. The insulation degrades with time and becomes weaker to sustain the PD events. The degradation changes the insulation property as a result of the electrical, mechanical and thermal stresses (Kuffel and Kuffel 2000). There are several types of PD in HV equipment such as internal, corona and surface discharges. According to (Montanari, Cavallini et al. 2006) (Zhang, Blackburn et al. 2007), internal discharge is more harmful than surface discharge and both are more harmful than corona discharge.

2.3.1 Internal Discharge

Internal discharge occurs in a defect of closed-volume within insulation material such as solid and liquid. The examples of the defect are void, cavity or delamination,

bubbles and cracks. This partial discharge (PD) is usually caused by the manufacturing process or in power cables accessories such as joints or terminations. In this type of PD, the electric field on the surrounding insulation is lower than the electric field inside the void. The property of the defect changes from non-conducting to conducting during PD incident, which results to a drop in the electric field within cavity from higher value to lower in a very short period of time (Illias 2011). It causes degradation to the insulation material when PD events repeat over time, which leads to breakdown. Figure 2.3 shows an internal discharge diagram.

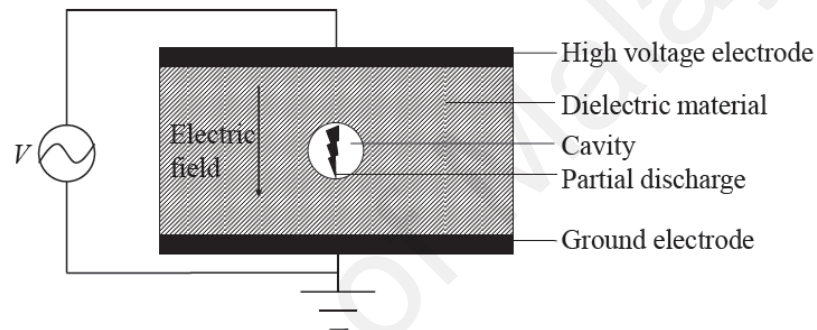


Figure 2.3: Internal discharge (Illias 2011)

2.3.2 Corona Discharge

Corona is also known as a glowing discharge when the air ionization at the conductor surrounding increases to a certain critical value caused by a voltage gradient (Jay and Goetz 1988). This discharge is shown in Figure 2.4. It will happen when the electric field at the sharp points exceeds the air breakdown strength. There are two types of corona, which are positive and negative discharge. The effects of corona are power loss in transmission line because of current is flowing out of the intended route, disturbing noise, radio interference and insulation deterioration. It is normally not considered a dangerous discharge but the behaviour of corona is the same as other types of PD and it can appear as a disturbance in online measurement (Ghaffarian Niasar 2012).

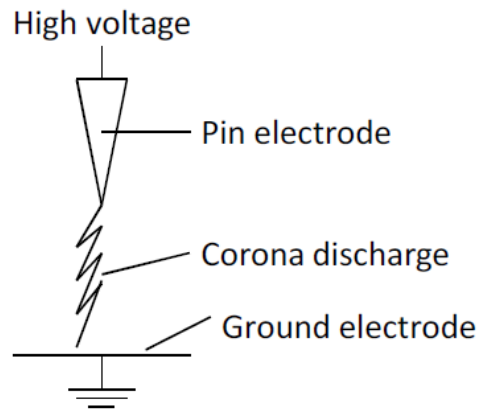


Figure 2.4: Corona discharge (Illias, Yuan et al. 2012)

2.3.3 Surface Discharge

Discharge that occurs on the insulation materials surface is called surface discharge, where the field at the tangent across the surface is high (Illias 2011). Difference in the source potential and ground electrode is bridged by this discharge through pollution paths or cracks on the insulation surface. Examples of surface discharge in the field is on the surface of insulating windings of HV cables or at the end of large generator stator windings (Edin 2001). Figure 2.5 shows an example of surface discharge.

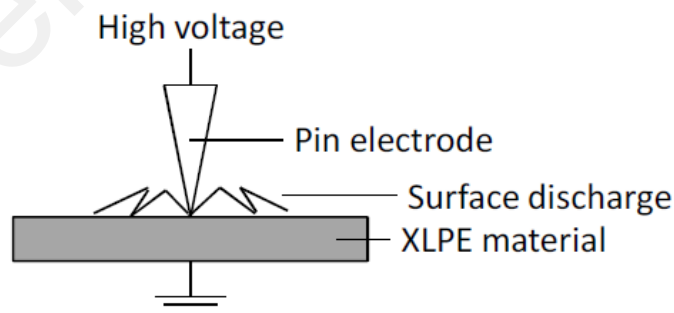


Figure 2.5: Surface discharge (Illias, Yuan et al. 2012)

2.4 Partial Discharge Measurement Methods

Measurement of PD is very important to monitor the insulation situation of high voltage (HV) apparatus. PD measurement has been used as a test to assess the design of

different insulation system and as a quality control test for the new equipment. In addition, the measurement of PD has been widely used for 20 years to diagnose insulation situation in electrical apparatus such as switchgear, transformers, cables, motors and generators (Stone 2005). In general, there are three important information regarding PD activities, which are detection, classification and location (Metwally 2004). It is important to have PD data along with details of the surrounding insulation materials to maintain or repair in a timely manner (Tenbohlen, Denissov et al. 2008). PD can be measured either online or offline. There are many methods that can be used to measure PD activity based on electrical or non-electrical phenomena. The most popular approaches of PD detection in HV power equipment are:

1. Optical measurement method
2. Acoustic measurement method
3. Chemical measurement method
4. Electrical measurement method

2.4.1 Optical Measurement Method

Optical measurement uses light during the presence of discharge. The light is disappearing in the ionization and excitation process form occurs due to partial discharge (PD). The emissions of light are affected by insulating medium and parameters such as temperature and pressure. Due to the opaque nature of mineral oil, this method is not recommended for a transformer (Sabat 2011). Figure 2.6 shows the arrangement of experimental test for optical method used to detect PD. The experiment setup is based on the concept of optical PD measurement as shown in Figure 2.7. The objectives is to identify and rectify localization in PD via optical measuring system inside of electrical equipment (Schwarz, Muhr et al. 2005).

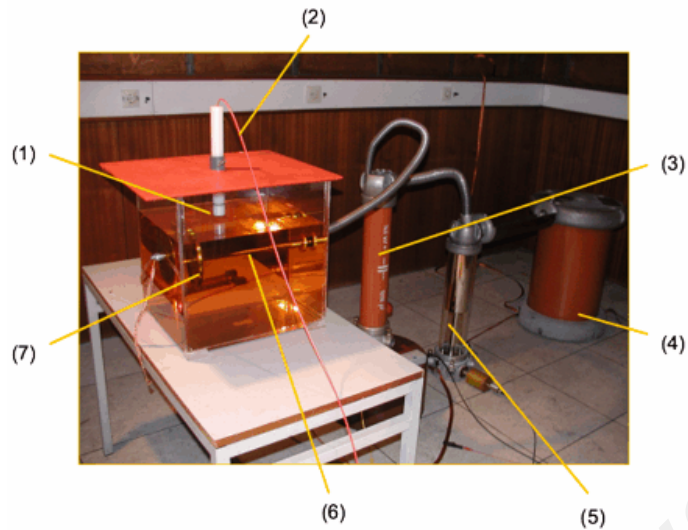


Figure 2.6: Experimental test setup; (1) Optical sensor, (2) Optical fibre, (3) Coupling capacitor, (4) High voltage supply, (5) Voltage divider, (6) Peak plate, (7) Oil container (Schwarz, Muhr et al. 2005)

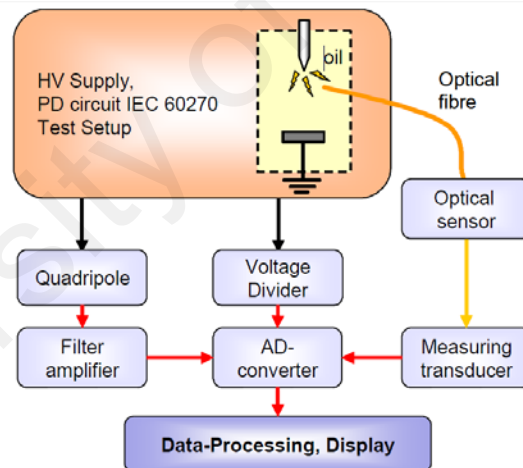


Figure 2.7: Theory of the optical PD measurement (Schwarz, Muhr et al. 2005)

The optical method uses a small, light in weight, very sensitive, high frequency response and significant immunity to electromagnetic interference (EMI) of optical fibre sensor. It can easily measure various chemical and physical parameters. In addition to PD detection and evaluation, (Greene, Tran et al. 1995), optical fibre acoustic sensors have been applied effectively in applications such as transportation observing, vehicle tracking water hydrophones and substance assets analysis (Furstenau, Schmidt et al.

1997). Due to the sensitivity of measurement, visual methods have limited use for detection of PD (Yaacob, Alsaedi et al. 2014).

2.4.2 Acoustic Measurement Method

Partial discharge (PD) is detected by an acoustic sensor for acoustic measurement method. This is based on the phenomena that PD produces sound. This sound can be heard or not, is made when the current streamer is formed and the evaporated material at the surrounding streamer. The rapid release of mechanical energy produced by the vapour spreads in the form of pressure field (Janus 2012). The acoustic detection system can be categorized in two, which are external and internal systems. The external system has a sensor outside of the high voltage (HV) equipment while the sensor locate inside power equipment is for the internal system to measure the wave pressure directly.

Highly sensitive piezoelectric film sensor is used by the acoustic technique as shown in Figure 2.8(a) and is formed as Figure 2.8(b). It has been applied to measure PD for HV equipment such as HV cables and power transformers. Piezoelectric film sensor is a crystal, which is in the form of disc at low resonant frequencies, where the resonances can be simply calculated (Cosgrave, Vourdas et al. 1993).

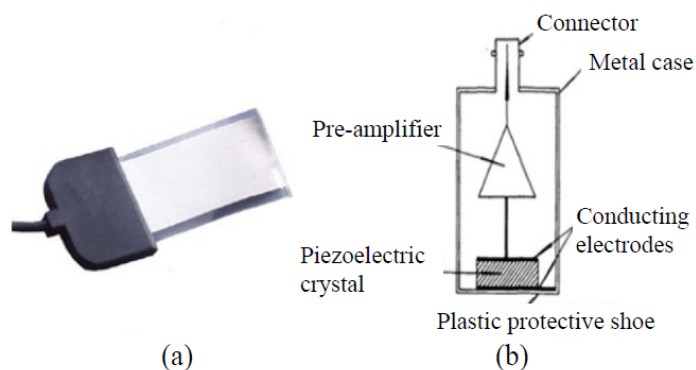


Figure 2.8: Acoustic sensor; (a) Sensor of piezoelectric film with connector, (b)

Standard scheme of the piezoelectric transducer sensor (Yaacob, Alsaedi et al. 2014)

This method is very effective in viewing and encoding acoustic signals generated during PD events. The main advantage of this method is it is unaffected by electromagnetic interference (EMI) (Sabat 2011) or in other words, it has better signal to noise ratio. On the other hand, the sensor can be placed at multiple places for PD detection, which can help to identify the PD types (Janus 2012). However, the acoustic method has disadvantage where the main problem is difficult properties of acoustic propagation route. This action is complicated to apply on non-homogeneous device, such as transformer. Acoustic method is usually used to find the location of insulation failure.

2.4.3 Chemical Measurement Method

A current streamer breakdown in the materials produces different chemical components during partial discharge (PD) activities. In this method, PD is chemically detected by observing the chemical changes (Sabat 2011). Dissolve gas analysis (DGA) and high performance liquid chromatography (HPLC) are the chemical measurement method tests practice today (Yaacob, Alsaedi et al. 2014). This test can be used only for oil filled components mainly on high voltage (HV) transformer (Janus 2012). Gases are produced when mineral oil breakdown and these gases are identified by DGA test. The level of different dissolved gases is taken from the oil sample during the test. The gases are mainly hydrogen and other gases such as ethylene, carbon oxide, carbon dioxide, methane and acetylene. (Janus 2012). This experiment shows the existence of PD and contributes extra data for the reason that of dissimilar level of each gas can be associated with certain type of error.

The side effect of breakdown in transformer wall insulation is measured by HPLC test for example the cellulose and its side effects. The disadvantages of using this test are degraded forms of glucose are not stable and the glucose level in oil is very small

(Bartnikas 2002) (Karmakar, Roy et al. 2009). There is no standard value of glucose concentration and it is related to fault (Janus 2012). This method does not have the evidence about the position of the PD and insulation damage. Hydrogen oil detector is shown in Figure 2.9. It can detect the hydrogen gas concentration in the transformer oil through the connection of two terminals, named semi-permeable membrane and hydrogen gas and then joined to a portable gas chromatograph. Portable gas chromatography allows the measurement of hydrogen gas concentration at intervals for several hours.

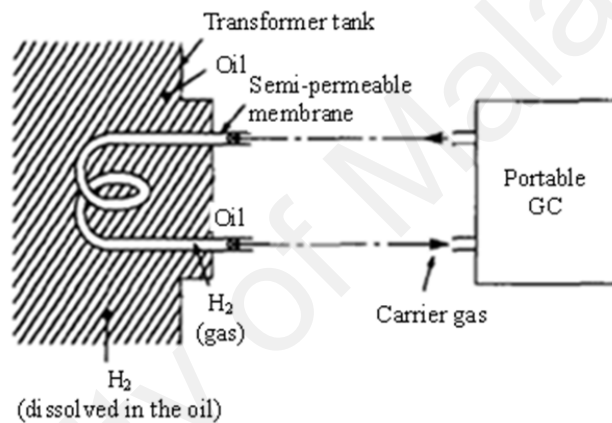


Figure 2.9: Hydrogen oil detector (Yaacob, Alsaedi et al. 2014)

For chemical measurement technique, sufficient dumped ancillary products or gas must be collected before the analysis can be initiated. Therefore, there are some delays between analysis and collection. This method is unsuitable for real-time monitoring and cannot detect the accurate location of PD sources. However, this technique has a good PD signals recording in laboratory situation and has a high sensitivity (Yaacob, Alsaedi et al. 2014).

2.4.4 Electrical Measurement Method

The most popular method used is electrical measurement in order to measure partial discharge (PD). Electrical detection is based on the pulse of electrical made by a current

streamer. There are two categories of electrical detection (Janus 2012). The first is direct probing, which use coupling capacitor connected to a test object and the second is the RF emissions, which uses antennas to detect PD. This research uses direct probing method as shown in Figure 2.10.

Figure 2.10 shows the circuit includes a high voltage supply (V), test object, coupling capacitor (C_k), coupling device, PD detector, USB controller and personal computer (PC). From the circuit diagram, PD detector and a coupling device are to detect PD signals from the test object. When a PD is detected, the raw data of PD signals are recorded and collected by a PC connected thru a USB controller for analysis (Illias, Yuan et al. 2012).

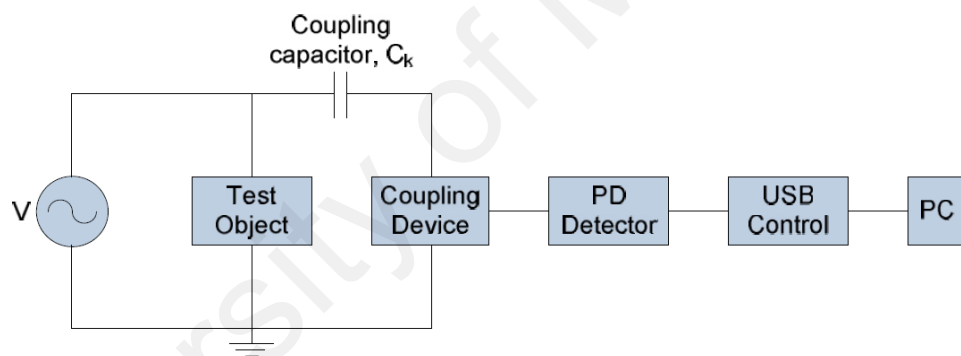


Figure 2.10: Direct probing method (Illias, Yuan et al. 2012)

Noise is the primary problem in this system because noise in the equipment causes PD false detection. Other than noise, this technique is challenging to apply on site, affected by electromagnetic interference (EMI) and false alarm because of its high sensitivity, inappropriate observing of transformers for a long term (Yaacob, Alsaedi et al. 2014). In this method, equipment is usually taken out for offline testing and energized by HV during testing. The advantages of this method are good PD signals recording in laboratory situation, sensitivity is high and very low signal attenuation

(Yaacob, Alsaedi et al. 2014) but the cost and time are very consuming although this method can provide the most accurate result (Janus 2012).

2.5 Previous Partial Discharge Classification Works

There are various works associated to the classification of partial discharge (PD), which have been done earlier. There are two classifier reviewed in this section, which are support vector machine (SVM) and artificial neural network (ANN).

2.5.1 Partial Discharge Classification using Support Vector Machine

In (Hao, Lewin et al. 2006), Hao et al investigated the performance of partial discharge (PD) sources using support vector machine (SVM) based on the various characteristics of parameter. The feature extraction methods used were wavelet decomposition coefficients, frequency spectrum and phase based information. Internal discharge, surface discharge in air, corona in air, corona in oil and floating discharge in oil are the types of PD sources to generate PD signals. For PD evaluation, a transformer bushing tap system was used as an investigation sample. The overall accuracy shows that frequency spectrum feature has the highest accuracy which is 98%.

In (Sharkawy, Mangoubi et al. 2007), the authors described the partial discharge (PD) recognition process for detecting and identifying transformer mineral oils polluted particles by using support vector machine (SVM). Estimated density function entropy and higher order moments were utilized as input features. More than 98% rate of accuracy was obtained by using 6 moments as input features as the moments by different combinations were tested.

In (Hao and Lewin 2010), the authors performed discrimination between different sources of partial discharge (PD). Corona discharge with distant earth, internal

discharge in oil and surface discharge in air are the types of PD artificial models. Wavelet analysis was utilized as the input characteristic. Only 2 samples were wrongly classified by using a support vector machine (SVM) as a classifier for out of 60 samples.

An experiment on three-phase paper insulated lead covered (PILC) distribution cable has been examined by (Hunter, Lewin et al. 2013) for investigating partial discharge (PD) produced by different defects. Three different defects of cable joint samples were studied which include spike on the ferrule, void in the crutch and on the top. Input features used were statistical characteristics that were combined with the features extracted with wavelet transform. The classification accuracy achieved was 91.1%.

Investigation on the characteristics of partial discharge (PD) measured from gas insulated substation (GIS) can be found in (Khan, Khan et al. 2014). Data collected at different SF₆ gas pressures with the size and position of the particle was classified by the support vector machine (SVM). Input feature of statistical was used and 94% of classification accuracy was obtained.

A gas insulated switchgear (GIS) simulator has been made by (Zhang, Xiao et al. 2014) in the laboratory. There are four typical insulation defects which are gas gap, free moving particles, metal needle and fixed metal particles. A combination of the characteristics of statistical and features extracted through the chaotic theory have been used as an input characteristic. A classifier of support vector machine (SVM) was used and meets the classification accuracy of 98%.

Support vector machine (SVM) was classified for partial discharge (PD) pattern in GIS (Ling, Bai et al. 2018). PD patterns categorized into four classes include floating electrode, surface discharge, corona discharge and particle discharge. Statistical features

were used as a feature extraction method and reaches above than 90% classification accuracy.

2.5.2 Partial Discharge Classification using Artificial Neural Network

Partial discharge (PD) classification of the earlier work has been reported in (Suzuki and Endoh 1992). The authors investigated PD pattern identification in 66kV cross-linked polyethylene (XLPE) cables and it was tested at 38kV AC by three-layer feed-forward back-propagation neural network (NN). The voltage of phase angle, pulse counts numbers and discharge magnitude were the input information for the NN. The NN classifier was classified 30 typical of input patterns and succeeds 90% accuracy value.

A multilayer neural network using the back-propagation algorithm was used in (Mazroua, Salama et al. 1993). In order to distinguish between discharge patterns, a cavity with dielectric electrodes and a cavity with metallic electrodes of discharges sources were employed. Apparent charge, fall time, rise interval, width and area PD pulse are the features used in this work. Test samples used are acrylic discs with different size and shape of artificial cavities. 20 measurements were applied for training and 10 for testing target for out of 30 measurements. 100% accuracy was achieved when distinguish different partial discharge (PD) pattern due to the shape of the cavity, but in differentiating cavity size only 60% was achieved.

A multilayer neural network was used in (Satish and Zaengl 1994) to identify 3D partial discharge (PD) forms. Test samples used were 7 specimens of different flat cylindrical void. A phase resolved partial discharge (PRPD) pattern was performed as feature extraction and 79% of accuracy was achieved. 73.85% with 5% noise and 42.2%

with 10% noise classification accuracy were achieved when a random noise was added to the pattern.

A system of multilayer neural network has been used in (Mazroua, Bartnikas et al. 1995) to differentiate between pulse shapes of the partial discharge (PD) by the electrical tree defect and cavities characteristic. The input features used to extract the PD signals were fall time, rise interval, peak amplitude, width and area pulse of PD. 94% of average accuracy classifying the different cavity sizes was achieved while for electric trees aging periods, 91% of average accuracy reached.

The use of two types of neural network, a modular neural network (MNN) and single neural network (SNN) have been studied in (Hong, Fang et al. 1996) for investigating the sources of partial discharge (PD). Test samples used consist of high voltage buses with a variety of defects initiated by different diameter of needle point. Average and maximum discharge magnitudes and PD pulse counts were used as the features vector of the PD signal. SNN achieved 88.31% accuracy while MNN achieved accuracy of 93.6%. They extended their research works in (Tao and Fang 2001) to show that MNN has higher training speed compared to SNN.

In (Lalitha and Satish 1998), Lalitha et al performed the compression of fractal image technique. Pulse count average, phase and magnitude spreads were used as the input features, which were trained by the neural network classifier. Surface discharges in air, multiple coronas in air, single point corona in air and cavity discharges were the partial discharge (PD) defect types. 100% classification accuracy achieved by 20% of the data while 80% of test sample data achieved 75% of classification accuracy.

Radial basis function neural network was utilized in (Lalitha and Satish 2000) to evaluate partial discharge (PD) patterns acquired from surface discharge, cavity

discharge and single point corona. Wavelet transforms feature was used as an input and more than 88% of accuracy was reached.

In (Karthikeyan, Gopal et al. 2005), Gopal et al explored probabilistic neural networks (PNN) for identification of partial discharge (PD) patterns. Insulation defects in PD data were identified by phase resolved partial discharge (PRPD) patterns. Corona in oil, corona in air and void were defect types and has been created by Perspex material. Statistical features used as the input feature vector of the PD pattern. As a higher quantity of test samples, a 100% accuracy of classification is achieved. In (Karthikeyan, Gopal et al. 2008), Gopal et al extended the researches by using a composite PNN.

The work presented in (Li, Sun et al. 2006) focuses on fractal and statistical features as input features practice with a back-propagation neural network (BPNN) classifier. Single point discharges in insulation oil, single point corona discharges in air, dielectric surface discharges in oil, dielectric surface discharges in air and discharges in cavity electrode system were artificial defect types. The results show that 88.44% accuracy reached by statistical features, 84.26% of accuracy achieved by fractal features and 93.64% accuracy achieved by combination of fractal and statistical.

Artificial neural network (ANN) has been researched by (Boczar, Borucki et al. 2009) for identifying partial discharge (PD) activity. Surface discharge, moving particles discharge in oil, multipoint plane discharge in oil with gas bubbles, multipoint surface discharge, point to plane in oil, point to point discharge in oil and point to point discharge in oil with gas bubbles, multipoint plane discharge in oil were artificial defects created. Power spectrum density method and short time Fourier transform were used as the input features. Up to 90% of classification accuracy was obtained.

Probabilistic Neural Network (PNN) was employed in (Evagorou, Kyprianou et al. 2010) through the wavelet packets transform as the input feature. Corona discharge in air, surface discharge in air, internal discharge in oil and floating discharge in oil were the artificial partial discharge (PD) categories. The outcomes acquired for surface discharge was 99.8%, the floating was 91.9%, 100% for the internal and 97.49% for the corona.

In (Venkatesh and Gopal 2011), Gopal et al proposed a Radial Basis Probabilistic Neural Network (RBPNN) for the partial discharge (PD) classification sources, which were void, void with air corona, oil corona and air corona. Feature extraction used in this work was Forward Orthogonal Least Square algorithm. Accuracy of classification between 80% and 90% was attained by RBPNN while 50% to 70% of accuracy was accomplished by PNN. In (Venkatesh and Gopal 2011), Robust Heteroscedastic Probabilistic Neural Network (RHPNN) has been applied and reached more than 90% of accuracy.

In (Gu, Chang et al. 2012), Gu et al proposed fractal feature characteristic for identification pattern of partial discharge (PD). Categories of deficiency for cross-linked polyethylene (XLPE) cable joints were recognized which included a healthy power cable, long outer semiconducting layer, artificial knife defect and short outer semiconducting layer in the XLPE insulation. 81.67% of accuracy rate was achieved by extension method and 73.33% accuracy rate was achieved by back-propagation neural network (BPNN) method, when 15% noise was applied. Characteristics of similar inputs and classifiers were used to classify the types of defect of high voltage transformer in (Chen, Gu et al. 2012).

RF antenna was used in (Shurrab, El-Hag et al. 2013) to identify partial discharge (PD) at the surface of insulating polymer under different conditions. Four cases were

reviewed, which includes corona from dead end, corona from energized end, surface discharge and combined PD. Features extraction of both spectral and statistical analyses have been applied and classification was performed using artificial neural network (ANN). The recommended method was successfully classifying types of PD with recognition accuracy in excess of 96%.

A modified artificial neural network recognized as ensemble neural network (ENN) was recommended in (Abubakar Mas'ud, Stewart et al. 2014) for classifying partial discharge (PD) patterns. Six PD faults were produced in research laboratory, which were corona in oil, surface discharge in air, electrode bounded void or cavity, corona in air, single void in polyethylene terephthalate (PET) and surface discharge in oil. Statistical features have been used as an input feature and 95% accuracy classification was obtained.

In (Li, Tang et al. 2015), Li et al presented two kinds of data pattern that were used as the input features of partial discharge (PD) signals namely, time resolved PD (TRPD) data and phase resolved PD (PRPD) data. A test sample of gas insulated switchgear (GIS) was used accompanied by the surface contamination, free particles, void in spacer and protrusion defects. Classifier of artificial neural network (ANN) has been used and achieved by 82.94% classification accuracy when using the TRPD data and 92% when using the PRPD data.

Artificial neural network (ANN) was utilized to classify PD source in HV equipment (Sukma, Khayam et al. 2018). Nine waveform parameters from each PD event were used for ANN classification. Four kinds of artificial PD sources, three types of noise sources by three types of sensors were used to generate waveform parameters in laboratory. The results show above than 90% of accuracy.

CHAPTER 3: PARTIAL DISCHARGE MEASUREMENT

3.1 Introduction

The methodology which is about the process involved in designing this project is described in this chapter. It includes the description of the project from the beginning until the end. It also discusses and states the steps used to perform this project. This part is to ensure that the objectives of the project are achieved.

3.2 Project Development

The experiment of partial discharge (PD) was performed in a high voltage (HV) enclosure cage in order to avoid any incident happens during experiment. Figure 3.1 shows a flowchart of PD classification used in this work. The samples of cable joint with artificial defects were prepared and PD measurement was investigated in the University of Malaya High Voltage Laboratory (UMHVL). Feature extractions were implemented to obtain the input features and applied as the input data for the classifiers. The process was repeated until the best technique was identified. The measurement was carried out at voltage lower than 9 kV. Each cable was energized at lower than 9kV and results of PD measurement were acquired. Each measurement of PD has an interval of around 60 seconds. Each sample was performed for a total of 100 signals. Therefore, a total of 300 PD signals for the three cable joint samples were acquired.

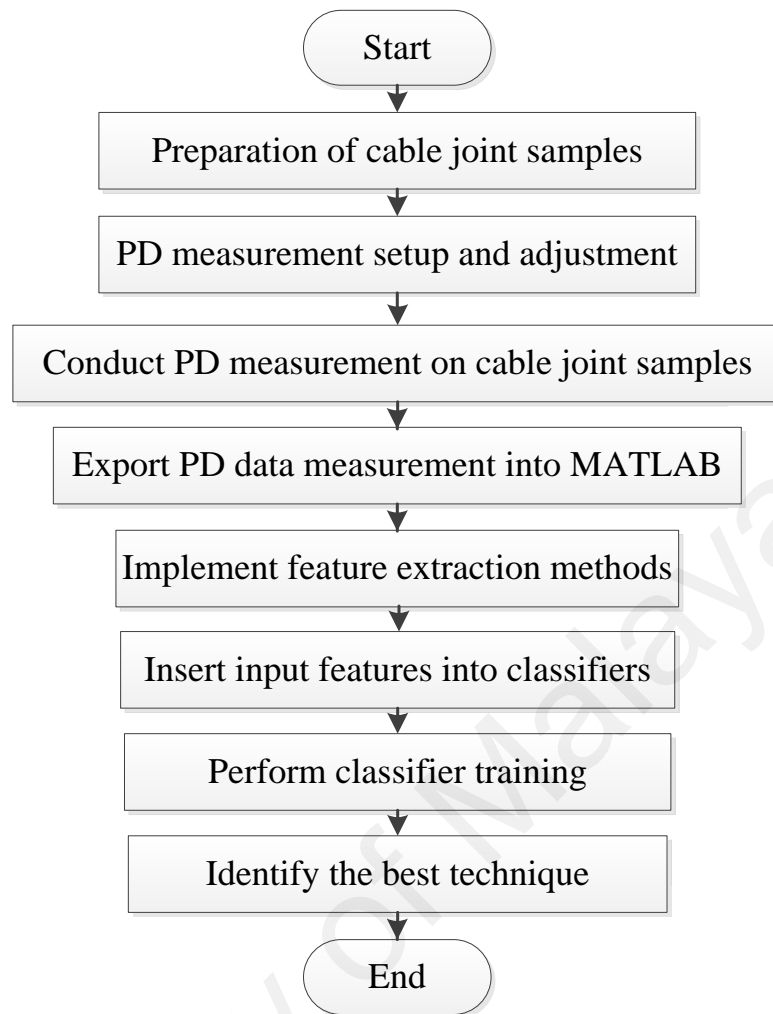


Figure 3.1: Flowchart of the project

3.3 Cable Joint Samples Preparation

Three cross-linked polyethylene (XLPE) cable joints of 11kV with a various artificial defects created were arranged in this work. 3 meters of cable length with a cable joint located in the centre was used from each sample. The lists of XLPE cable joint samples are presented in Table 3.1. Damage to insulation of incision was produced by making shallow cut on a layer of XLPE with sharp knife. Damage along the axis direction of shift was created by including the angle of cables, which is from the off centre. Defect of tip in semiconductor layer was introduced by creating a rough edge in the semiconductor. All defects have been made at XLPE cable joints before installed. Figure 3.2 shows the pictures of the cable defects.

Table 3.1: Samples of XLPE cable joints defects

Cable Joint	Defect Type
C1	Defect of incision in insulation
C2	Defect of shift in axial direction
C3	Defect of tip in semiconductor layer



(a)



(b)



(c)

Figure 3.2: Defects created; (a) Insulation incision defect, (b) Axial direction shift defect, (c) Semiconductor layer tip defect

3.4 Partial Discharge Measurement Setup

The schematic diagram of a partial discharge (PD) measurement system under AC voltage is shown in Figure 3.3 and the actual measurement setup in high voltage (HV) laboratory is presented in Figure 3.4. The test setup includes a step-up transformer, which is the source of HV, measuring capacitor, which is used to calculate the operating voltage, test objects, coupling capacitor, coupling devices, PD detector and a USB controller that is attached to the personal computer (PC). Coupling device changes the current detected to the voltage. The PC was used to configure the settings of PD detector and store data measured. In this work, Mtronix MPD600 issued by Omicron was used to measure the PD.

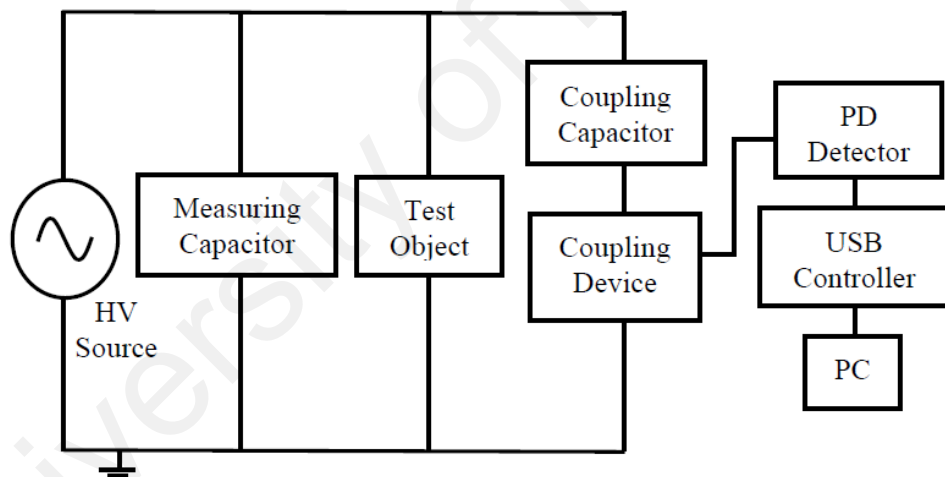


Figure 3.3: Configuration of PD measurement under AC voltage

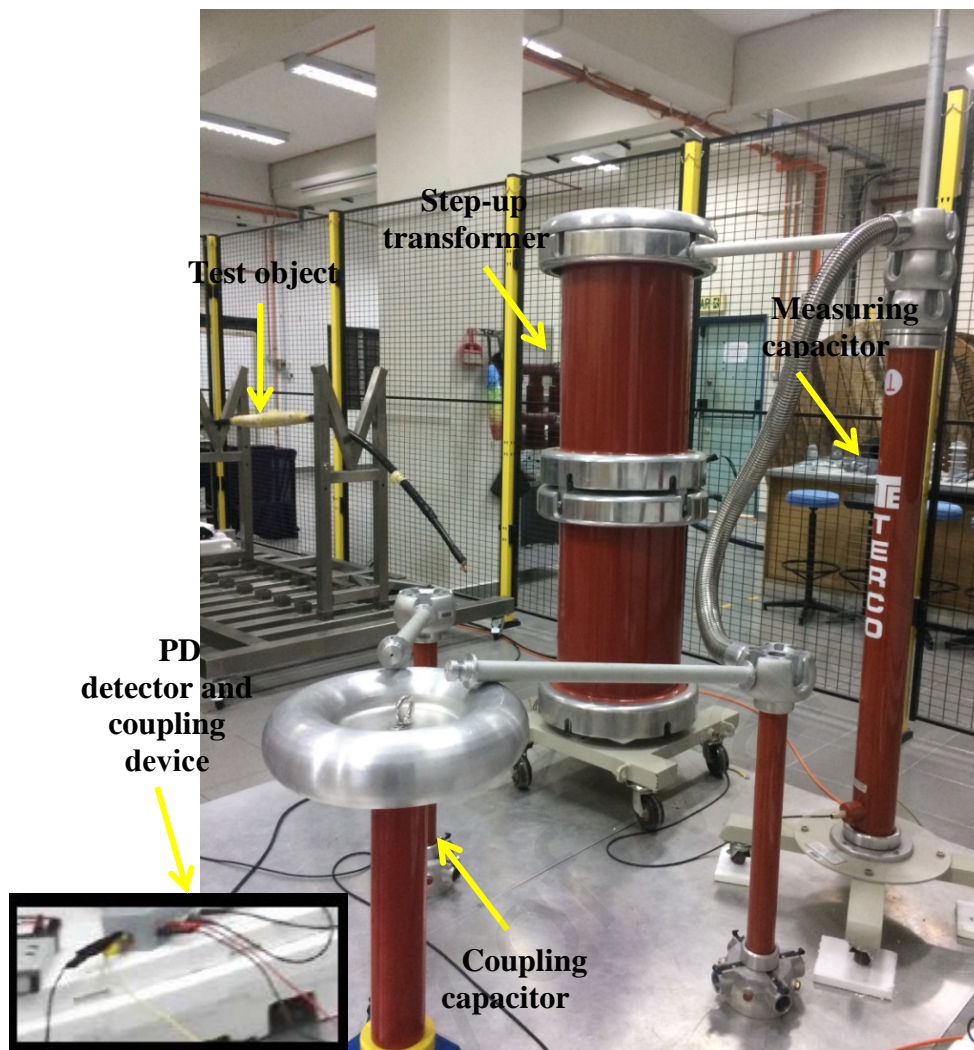


Figure 3.4: PD measurement setup in HV laboratory

The test object for each PD type was connected to a HV supply. The supply voltage was controlled by a power bench as shown in Figure 3.5. The coupling capacitor was coupled to the test object and the PD detector. The measuring circuit must be calibrated before conducting all measurement. The calibration was performed by calibrator CAL 542. The raw PD signals data were recorded in ‘.csv’ file format in Microsoft Excel, which were captured by a 2.5GHz digital oscilloscope, LeCroy WR625zi. For each PD type, 100 signals were recorded and saved into the PC for data analysis.



Figure 3.5: Power bench in HV laboratory

From the PD signals obtained, features were extracted using statistical features and principle component analysis (PCA) after discrete Fourier transform (DFT), discrete wavelet transform (DWT) and wavelet packet transform (WPT) signal processing techniques were performed. These features were used as the input data for support vector machine (SVM) and artificial neural network (ANN) to classify the types of defect. The optimum parameters of the SVM and ANN were determined by testing with different parameters. The accuracy results of each method were compared with each other to identify the best method which yields the highest accuracy of classification percentage.

3.5 Partial Discharge Feature Extractions

This section explains different analysis and classification techniques for partial discharge (PD). Feature extraction means altering existing characteristics to dimensions that are useful for feature reduction to avoid redundancy as a result of high dimensional data (Subasi and Ismail Gursoy 2010). This feature was obtained from the analysis technique and utilized as the input for classification process. It is compulsory to apply feature extraction process to obtain the input feature for classification of PD (Ma, Chan et al. 2013). The extracted input feature is used to train the PD classifier. Two different

features were utilized in this work to obtain the input from PD data, which include statistical features and principle component analysis (PCA). Three different signal processing techniques were applied, discrete Fourier transform (DFT), discrete wavelet transform (DWT) and wavelet packet transform (WPT). These input features were used to train and test the support vector machine (SVM) and artificial neural network (ANN) to classify defect types.

3.5.1 Statistical Features

In (Gulski 1993), Gulski used statistical parameters and this concept was introduced as partial discharge (PD) analysis tool in the early nineties (Lai, Phung et al. 2010). The four moments of standard statistical are mean (μ), standard deviation (σ), skewness (Sk) and kurtosis (Ku) (Kreuger, Gulski et al. 1993) (Press, Press et al. 1989, Devore 2011). The first moment is mean value, which used as a distribution center of mass. It is the average value of a random variable X , the most important characteristics of its distribution (Soong 2004). The second moment is variance, which measures the spread or dissemination of random variables X about the mean.

The third moment is skewness, which is defined mathematically as the average cubed deviation from the mean divided by the cubed standard deviation. Skewness is the level of asymmetry distributions taking into account the normal distribution (Raymond and Illias 2017). If the skewness is greater than zero, it means the distribution is positively skewed. If it is less than zero, the distribution is negatively skewed and if the skewness is zero, the distribution is symmetrical. Figure 3.6 illustrates the condition of the third moment. Figure 3.6 (a) shows a positively skewed distribution, where the distribution is not symmetrical with a larger left side, Figure 3.6 (b) shows a symmetrical distribution where the mode, median and mean is at the center and Figure 3.6 (c) shows a negatively

skewed distribution, where the distribution is not symmetrical with a bigger right side (James and Phung 1995).

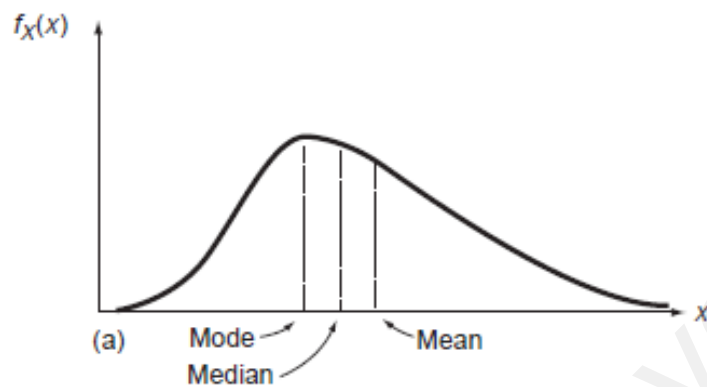


Figure 3.6 (a): Positively skewed distribution

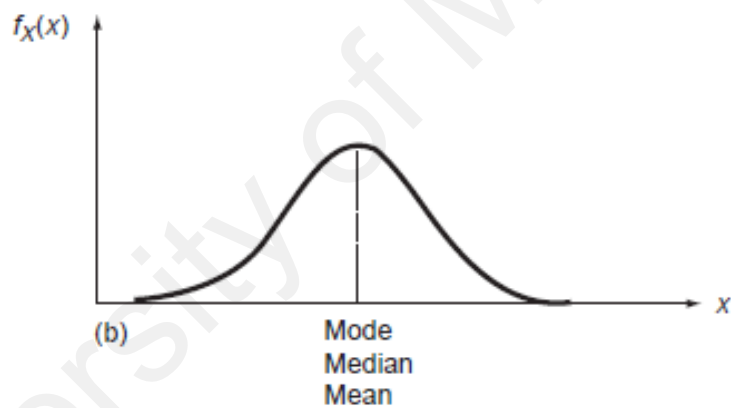


Figure 3.6 (b): Symmetrical distribution

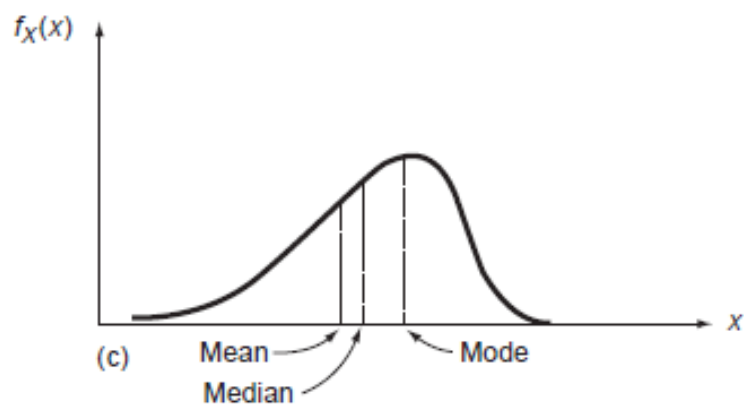


Figure 3.6 (c): Negatively skewed distribution

The fourth moment is known as kurtosis. Kurtosis is an indication for a sharp distribution. If the distribution has the same sharpness as a normal distribution, the kurtosis is equal to three. Hence, the kurtosis is calculated based on that value which is higher or lower than three. Figure 3.7 shows distribution when the kurtosis equals to 3, which is called mesokurtic (normal). For kurtosis more than 3, the distribution is called leptokurtic (sharper distribution) while platykurtic (flatter distribution) is for kurtosis less than 3.

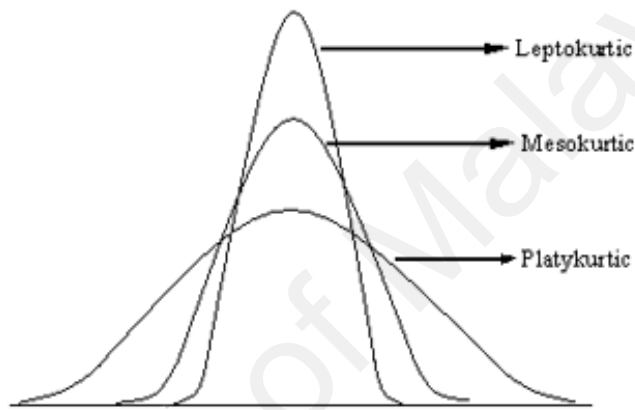


Figure 3.7: Positive, negative and normal kurtosis

The mean, standard deviation, skewness and kurtosis are calculated as follows (Sahoo, Salama et al. 2005) (Kreuger, Gulski et al. 1993):

$$\text{Mean: } \mu = \frac{\sum_{i=1}^N x_i f(x_i)}{\sum_{i=1}^N f(x_i)}$$

$$\text{Standard deviation: } \sigma = \sqrt{\frac{\sum_{i=1}^N (x_i - \mu)^3 f(x_i)}{\sigma^3 \sum_{i=1}^N f(x_i)}}$$

$$\text{Skewness: } S_k = \frac{\sum_{i=1}^N (x_i - \mu)^3 f(x_i)}{\sigma^3 \sum_{i=1}^N f(x_i)}$$

$$\text{Kurtosis: } K_u = \frac{\sum_{i=1}^N (x_i - \mu)^4 f(x_i)}{\sigma^4 \sum_{i=1}^N f(x_i)} - 3.0$$

where $f x_i$ is interest function, x_i is distribution discrete values and N is data size .

3.5.2 Principle Component Analysis

Principle component analysis (PCA) is a reduction data process that stores data information in space reduced by loss-lack of information (Raymond and Illias 2017). This can change data from one dimension of high to a low dimension. This is completed by projecting data at a direction with the biggest variance at lower dimension. It will maximize the scatter of the projected samples (Harbaji, Shaban et al. 2015). By solving this Eigen problem, this linear subspace can be found by (Harbaji, Shaban et al. 2015) (Jing and Hou 2015):

$$cov(X)M = \lambda M$$

where $cov(X)$ is the covariance matrix of the dataset X , M is a linear mapping created by the d principle eigenvectors of the covariance matrix and λ are the d principal eigenvalues. The low-dimensional data y_i of the data points x_i are calculated using linear mapping:

$$Y = XM$$

The feature sets will be produced by the elements of Y (Ma, Chan et al. 2013). The matrix covariance is able to determine which direction contains the most significant difference in the dataset, making a practical tool for an option of a subset of the features. The most significant concern in PCA is the quantity of component principles needed to obtain a precise representation of the original data. The best number of major components to represent the best data is by using the scree plot. A Scree plot is a graph of Eigen value versus the number of magnitude. The amount of the best is selected at

the point where the graph has a sudden change in slope, where the slope on the left side is higher than the right side (Babnik, Aggarwal et al. 2007).

3.6 Partial Discharge Signal Processing Techniques

Raw data need to be processed using signal processing tools in order to optimize the classification analysis of partial discharge (PD) measurement. The purpose of signal processing is to remove the unwanted noise. In this project, raw PD signals are processed by three different techniques of signal processing, which include discrete Fourier transform (DFT), discrete wavelet transform (DWT) and wavelet packet transform (WPT).

3.6.1 Discrete Fourier Transform

Fourier transform is one of the tools that can be used to analyse the frequency component of the signal. The purpose of Fourier transform is converting a time domain signal into a frequency component (Gonzalez and Woods 2002). However, Fourier transform cannot tell at what instance the particular frequency rises over the whole time axis. The sliding window, which can give information of time and frequency, is used in order to find the spectrogram, which is the Short Time Fourier Transform or Fast Fourier Transform (FFT). Spectral analyses identify the frequency component in the data. Signal of discrete Fourier transform (DFT) is simply a discrete-time data set converted to discrete-frequency representation. DFT is obtained using (Gonzalez and Woods 2002):

$$F[n] = \sum_{k=0}^{n-1} f[k]e^{-j\frac{2\pi}{N}nk} \quad n = 0 : N - 1$$

All work was done by using MATLAB software. The function 'fft' which is the fast Fourier transform in MATLAB was used to compute DFT. The input data vectors were considered as a window length by using 'fft' function. The computed DFT is the output and is called transform length. Distinction between window length ($m = \text{length } x$) and the transform length ($n = \text{length } y$) were made by FFT algorithm. The input data was chopped by FFT algorithm in order to achieve the desired transformed length. Theoretically, the DFT converts the raw partial discharge (PD) signals into discrete-frequency representation. The extracted signals are then trained and tested by the support vector machine (SVM) and artificial neural network (ANN).

3.6.2 Discrete Wavelet Transform

Wavelet means small wave. Wavelet analysis is similar to Fourier analysis, which breaks a signal down into its component parts for investigation (Chan 2012). Wavelet transform can give information in both time and frequency domains. Fast Fourier transform uses sliding window that can give information of both frequency and time. However, the problem is the length of the result window resolution limits the frequency. Hence, wavelet is the solution for this problem. Figure 3.8 and Figure 3.9 show comparison between sine wave signal and the wavelet signal respectively. From this figure, the signal of sine wave is smooth and has infinite length. Wavelet is irregularly and compactly supported so that wavelet is an appropriate tool to analyse the signal of a non-stationary. A discontinuity or sharp change can be analysed by its irregular shape. A temporal localization of signal features can be enabled with their compact support natures.

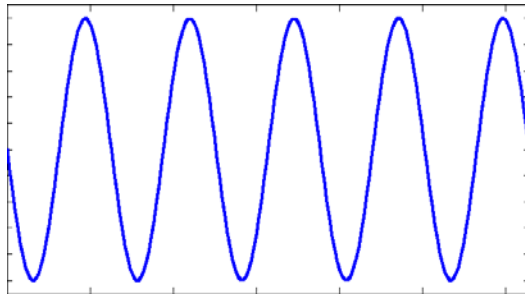


Figure 3.8: Sine wave signal

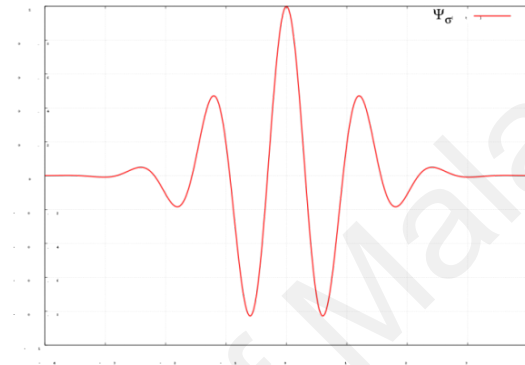


Figure 3.9: Wavelet signal

Discrete wavelet transform (DWT) was used in this work, which is the method for signal de-noising (Stone 2005). DWT is defined as (Salomon 2004):

$$W_{j,k} = \sum_{n \in \mathbb{Z}} \varphi(n) 2^{\left(-\frac{j}{2}\right)} \psi(2^{-j}n - k)$$

where $\varphi(n)$ is discrete function of signal, j and k are integers.

DWT was used to extract relative characteristics of partial discharge (PD) which vary according to types of PD (Evagorou, Kyprianou et al. 2010). DWT is a process of filtering and down sampling signal, and decomposes into two coefficients associated with frequency components. They are approximations (A), owned by low frequency and detail (D) for high frequency (Pylarinos, Siderakis et al. 2011). The signal decomposition continues producing approximate and detail coefficients from the earlier

approximate coefficient according to the levels number of the wavelet family that have been selected. The second stage of DWT is to restructure the original signal by according to the inverse discrete wavelet transform (IDWT) from the last approximate coefficient backward by up sampling and filtering.

Figure 3.10 shows the dilation function of the DWT. DWT is characterized as a tree of low pass filter and high pass filter. For DWT, each step is transformed thru a low pass filter. The low pass filter decomposes an original signal into a component of lower resolution. In this case, a high pass filter is not analysed further. The input size of the data to be analyses decides the maximum number of the dilation.

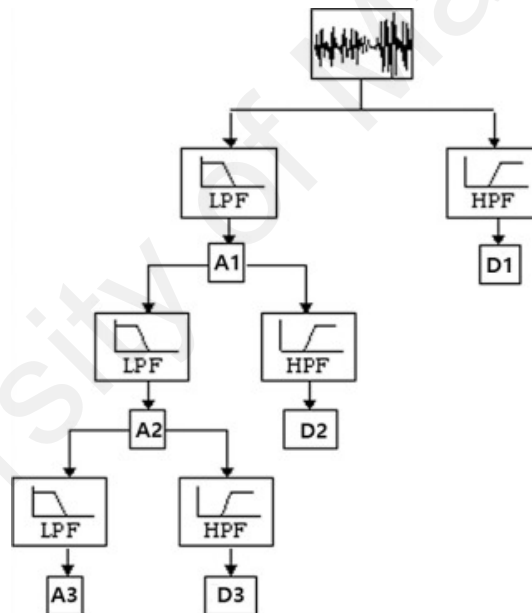


Figure 3.10: DWT dilation representation (Chan 2012)

The 'dwt' command of single dimensional wavelet decomposition with respect to the particular wavelet ('wname') was used in MATLAB for DWT. All 100 signals data for each defect types were computed and extracted for approximation and the details coefficients. Artificial noise was added into the signal. The extracted signals were then trained and classified by the support vector machine (SVM) and artificial neural network (ANN).

3.6.3 Wavelet Packet Transform

Wavelet packet transform (WPT) is the same as discrete wavelet transform (DWT) in the sense of the use of wavelet (Chan 2012). The advantage of using WPT compared to DWT is wavelet packet utility decomposes both high frequency and low frequency components. This is also called the approximations (low frequency) and details (high frequency). Figure 3.11 shows a WPT dilation representation. From Figure 3.11, the original signal is decomposed through low-pass filter and high-pass filter for approximations and details components. A is the approximation (low-pass) component and D is the detail (high-pass) component. This can significantly increase the versatility and the power of DWT. WPT framework of de-noising and compression is same as the wavelet framework. The different is wavelet packet offers more complex and flexibility analysis (MATLAB). This is due to the approximations and the details coefficients are analysed separately.

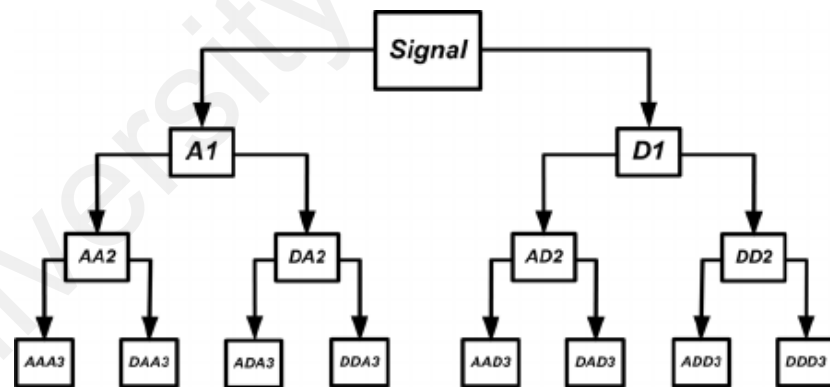


Figure 3.11: WPT dilation representation

Figures 3.10 and Figure 3.11 show the difference of wavelet framework and wavelet packet. In wavelet analysis, the approximations and the details are split. The approximations are then divided again by itself into the second level and details. This process will be repeated to the desired n-level. In wavelet packet analysis, decomposition is more complex. The entropy-based criterion helps the complexity of

the process. This entropy-based criterion looks at each node of the decomposition tree and the quantity information to be gained. Hence, the best wavelet tree can be found by entropy-based criterion. The extracted signal then trained and classified by the support vector machine (SVM) and artificial neural network (ANN).

3.7 Partial Discharge Classifiers

Two intelligent classifiers were applied in this research work, support vector machine (SVM) and artificial neural network (ANN). These classifiers were trained and classified the types of defect for the samples of three cross-linked polyethylene (XLPE) cable joints.

3.7.1 Support Vector Machine

Support vector machine (SVM) is the artificial intelligence method widely used for classification activities. SVM was firstly established by V. N. Vapnik in 1995 as a theory of statistical learning applications (Hunter, Hao et al. 2010) that can handle complex pattern classification problem. SVM maps data to the higher dimensions by using the linear classification (de Oliveira Mota, da Rocha et al. 2011). The structure of decision function results in a set of labelled training data. Figure 3.12 shows the operation of SVM as continuity to the problem of optimal hyperplane.

From Figure 3.12, 'm' is a separating margin. This hyperplane is in between the separable of two linear data classes. The biggest separating margin 'm' between the hyperplane and data points is the optimum solution by the SVM (Ab Aziz, Hao et al. 2007). The function of the hyperplane of each training data point will be iteratively optimized by the SVM. The data point closest to the margin is called support vectors. The parameter optimization is completed when the models were produced from the training data set. The labelled training data set generates the SVM algorithm. The

optimal hyperplane is constructed to classify the two different classes. Depth works of mathematical modelling and learning algorithm can be searched in (Ab Aziz, Hao et al. 2007).

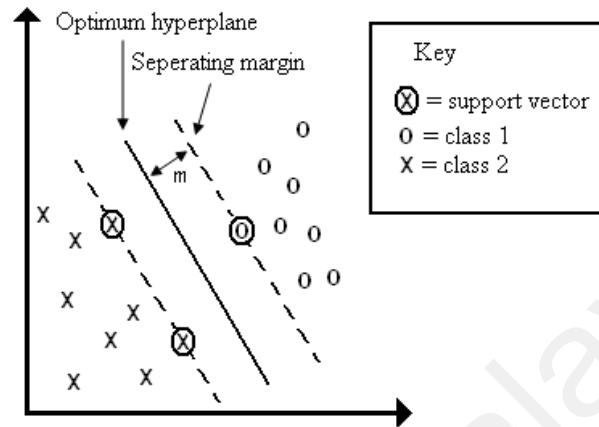


Figure 3.12: Optimum hyperplane diagram (Hunter, Hao et al. 2010)

SVM initially intended to deal with cases of linearly separable, but not all problems are linearly separated. SVM linear classifier as a conventional will not work effectively when conduct with non-linear problems. Therefore, a kernel technique was applied to handle non-linear problems using multiple linear classifier (Ab Aziz, Hao et al. 2007). SVM can be enhanced to several domains and tasks using kernel method based on the selection of basic algorithm and function of the kernel. It solves problem before linear mapping has higher dimensions. This can reduce dimensions problems to get the smallest feature set that delivers information. Therefore, the use of kernel method will keep off the dimensions curse (Jing and Hou 2015).

3.7.2 Artificial Neural Network

Artificial neural network (ANN) is suitable for partial discharge (PD) classification because it has good generalizing capabilities, flexibility, adaptability (Meruelo, Simpson et al. 2016) and not affected by small input changes. ANN can make the right decision

even though the input has slightly changed compared to the input used in the training session. This is important for PD classification where the PD patterns always have several variation even for the same source of defect (Mazroua, Salama et al. 1993). The network architecture will determine the ANN model, such as activation function (transfer function) and learning algorithm.

The learning algorithm reveals about how the neural network adjust its weights for the given training vectors. The activation function described the neurons connection. The activation function can be a linear or non-linear function and it calculates the output vector of neuron to the given input vector. When there is a sufficient activation, the neurons hold an output of '1' and '0' where it is not. The most standard activation function used in multilayer networks, which is trained using the back-propagation algorithm, is sigmoid function as shown in Figure 3.13 (Michael 2005):

$$f(x) = \frac{1}{1 + e^{-x}}$$

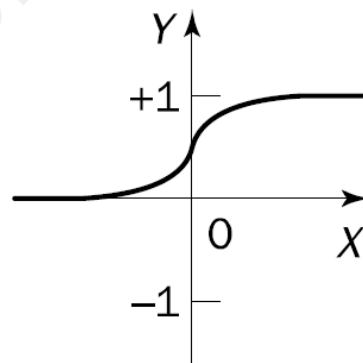


Figure 3.13: Sigmoid function (Michael 2005)

There are two popular ANN, namely Kohonen self-organizing mapping and multilayer feed-forward neural network, which trains through back-propagation algorithm (Lek and Guégan 1999). In general, ANN is composed of neurons primarily arranged to three layers (Satish and Zaengl 1994) (Illias, Chai et al. 2015). Each layer in

ANN is fully connected to the following layer. The first layer is called the input layer, which basically accepts the data subject to be analysed. The second layer is called hidden layer, which has no direct contact with the outside. The third layer is called the output layer, which gives network performance results based on the data entered in the first layer (Boyle 2011). For the purpose of PD classification, the minimum of two input features are necessary during training to avoid divergence (Jin, Chang et al. 2006). Figure 3.14 shows a typical feed-forward network with a single hidden layer which comprises three nodes, five input neurons and one output.

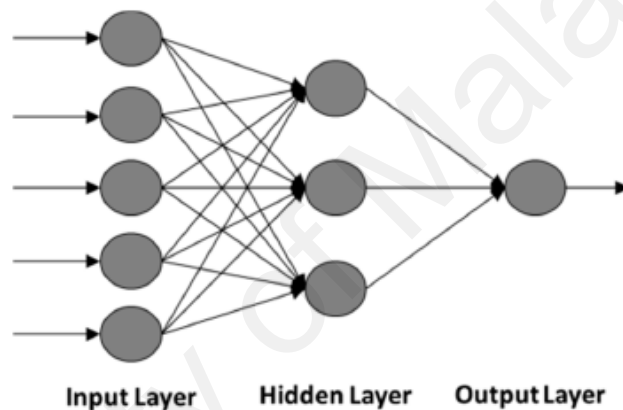


Figure 3.14: Feed-forward network (Corte-Valiente, Castillo-Sequera et al. 2017)

Learning standard in ANN that is commonly used is the feed-forward back-propagation neural network (BPNN) (Gençoğlu and Cebeci 2009), where it is a supervised learning network trained in a process of backward forward. Biases and weights are initialized into random small values through the forward process. Vector features owned by correlating sample is then applied to calculate the output of neurons in each layer using function activation threshold that can use different functions (Majidi and Oskuoee 2015). The disadvantages of the BPNN are longer time of convergence and the tendency for training failure (Mas'ud, Albarracín et al. 2016). Depth works of mathematical modelling and learning algorithm can be searched in (Mazroua, Salama et al. 1993) (Al-geelani, Piah et al. 2015) (Majidi, Fadali et al. 2015).

CHAPTER 4: RESULTS AND DISCUSSIONS

4.1 Introduction

This section discusses the results of three cross-linked polyethylene (XLPE) cable joints defects using partial discharge (PD) measurement approach. PD measurement can check the insulation quality of cable joints by detecting the condition and type of defect. The result of PD measurement was performed offline on cable systems. The features extraction was used as the input to the support vector machine (SVM) and artificial neural network (ANN) classifiers. The input features are the mean, standard deviation, kurtosis and skewness as statistical features and principle component analysis (PCA). Discrete Fourier transform (DFT), discrete wavelet transform (DWT) and wavelet packet transform (WPT) were applied as the signal processing techniques.

SVM and ANN classifiers were used to classify the defect types. The classification of PD was performed by using MATLAB program. 100 extracted data for each defect types of PD was used as an input for the ANN and SVM classifiers. ANN and SVM were trained and tested to classify the defect types. The results are shown by the ANN and SVM accuracies. In order to obtain the best result, the program was run for three times. The overall accuracy of the ANN and SVM that has the highest accuracy is chosen to obtain the final result for every signal processing method.

4.2 Classification Results by Support Vector Machine

Before analysing the partial discharge (PD) data, the raw data of PD signals need to be extracted first. Each PD signal was tested for a clean PD signal and by adding noise. The signals were added with noise, resulting in signal-to-noise-ratio (SNR) of 1, 20, 40, 60 and 80dB. After the input signals was extracted by discrete Fourier transform (DFT), discrete wavelet transform (DWT) and wavelet packet transform (WPT), the signals

were trained and tested by support vector machine (SVM) to classify the defect types using MATLAB programming. The best results are shown by the highest accuracy value.

4.2.1 Statistical Features with Discrete Fourier Transform

Table 4.1 shows SVM accuracy for mean feature with DFT signal at different SNR. For defect 1, the accuracy reading shows 100% from SNR = 1 to SNR = 100. For defect 2, the reading shows 96.6667% accuracy for SNR = 1 and then increases to 100% accuracy from SNR = 20 to SNR = 100. The accuracy reading shows zero values for SNR = 1 and SNR = 20 and increases to 3.3333% for SNR = 40 to SNR = 100 for defect 3 accuracy. Defect 1 has the highest accuracy reading followed by defect 2 while defect 3 has the lowest accuracy value. Hence, defect 1 and defect 2 can be classified correctly by SVM but cannot classify defect 3 correctly by using mean feature.

Table 4.1: SVM accuracy for DFT-mean

SVM ACCURACY (%)						
Defect	Signal-to-noise-ratio (SNR)					
Accuracy	1	20	40	60	80	100
1	100	100	100	100	100	100
2	96.6667	100	100	100	100	100
3	0	0	3.3333	3.3333	3.3333	3.3333
Average	65.5556	66.6667	67.7778	67.7778	67.7778	67.7778

Table 4.2 shows SVM accuracy reading for standard deviation feature with DFT signal at different SNR for different defect type. For defect 1, the accuracy reading shows 100% from SNR = 1 to SNR = 100. For defect 2, the accuracy reading is not

changed from SNR = 1 to SNR = 100, which was 96.6667%. The accuracy reading shows zero values for SNR = 1 to SNR = 100 for defect 3 accuracy. Defect 1 and defect 2 have the highest accuracy reading. Hence, defect 1 and defect 2 can be classified correctly by SVM but cannot classify defect 3 correctly by using standard deviation feature.

Table 4.2: SVM accuracy for DFT-standard deviation

SVM ACCURACY (%)						
Defect Accuracy	Signal-to-noise-ratio (SNR)					
	1	20	40	60	80	100
1	100	100	100	100	100	100
2	96.6667	96.6667	96.6667	96.6667	96.6667	96.6667
3	0	0	0	0	0	0
Average	65.5556	65.5556	65.5556	65.5556	65.5556	65.5556

Table 4.3 shows SVM accuracy reading for kurtosis feature with DFT signal at different SNR for different type of defect. For defect 1, the accuracy reading shows 66.6667% for SNR = 1. Then, the reading of accuracy decreases from 66.6667% to 63.3333% for SNR = 20 to SNR = 100. For defect 2, the accuracy reading shows zero values for SNR = 1 until SNR = 100. The accuracy reading shows 100% for SNR = 1 until SNR = 100 for defect 3 type. Defect 3 has the highest accuracy reading which is 100% accuracy compared to defect 1 which is 66.6667% and 63.3333%. However, defect 2 has the lowest accuracy which is zero. Hence, defect 1 and defect 3 can be classified correctly by SVM but cannot classify defect 2 correctly by using kurtosis feature.

Table 4.3: SVM accuracy for DFT-kurtosis

SVM ACCURACY (%)						
Defect Accuracy	Signal-to-noise-ratio (SNR)					
	1	20	40	60	80	100
1	66.6667	63.3333	63.3333	63.3333	63.3333	63.3333
2	0	0	0	0	0	0
3	100	100	100	100	100	100
Average	55.5556	54.4444	54.4444	54.4444	54.4444	54.4444

Table 4.4 shows SVM accuracy reading for skewness feature with DFT signal at different SNR. For defect 1, the accuracy reading shows 66.6667% for SNR = 1. Then, the reading of accuracy decreases from 66.6667% to 63.3333% for SNR = 20 until SNR = 100. For defect 2, the accuracy reading shows zero values for SNR = 1 until SNR = 100. The accuracy reading shows 100% for SNR = 1 until SNR = 100 for defect 3 type. Defect 3 has the highest accuracy reading which is 100% accuracy compared to defect 1 which is 66.6667% and 63.3333%. However, defect 2 has the lowest accuracy which is zero values of reading. Hence, defect 1 and defect 3 can be classified correctly by SVM but cannot classify defect 2 correctly by using skewness feature.

Table 4.4: SVM accuracy for DFT-skewness

SVM ACCURACY (%)						
Defect Accuracy	Signal-to-noise-ratio (SNR)					
	1	20	40	60	80	100
1	66.6667	63.3333	63.3333	63.3333	63.3333	63.3333
2	0	0	0	0	0	0
3	100	100	100	100	100	100
Average	55.5556	54.4444	54.4444	54.4444	54.4444	54.4444

Table 4.5 shows SVM accuracy average reading of statistical features with DFT signal processing technique. For mean, SVM accuracy average reading shows increased from 65.5556% to 66.6667% for SNR = 1 and SNR = 20 respectively. From SNR = 20 to SNR = 40, the accuracy average reading also shows slight increase from 66.6667% to 67.7778%. Then, the accuracy average reading is maintained at 67.7778% for SNR = 40 until SNR = 100. For standard deviation feature, the accuracy average reading shows 65.5556% which was not changed from SNR = 1 until SNR = 100. Kurtosis and skewness features have the same accuracy average reading. The reading decreases from 55.5556% to 54.4444% from SNR = 1 to SNR = 20, then the reading was maintained from SNR = 20 to SNR = 100 which is 54.4444% accuracy. Figure 4.1 shows SVM accuracy average reading at different SNR for DFT signal processing technique. The figure shows that mean has the highest accuracy average reading among the other statistical features, which is 67.7778% while kurtosis and skewness have the lowest accuracy.

Table 4.5: SVM accuracy average reading for DFT signal

SVM ACCURACY (%)						
Statistical Features	Signal-to-noise-ratio (SNR)					
	1	20	40	60	80	100
Mean	65.5556	66.6667	67.7778	67.7778	67.7778	67.7778
Standard deviation	65.5556	65.5556	65.5556	65.5556	65.5556	65.5556
Kurtosis	55.5556	54.4444	54.4444	54.4444	54.4444	54.4444
Skewness	55.5556	54.4444	54.4444	54.4444	54.4444	54.4444

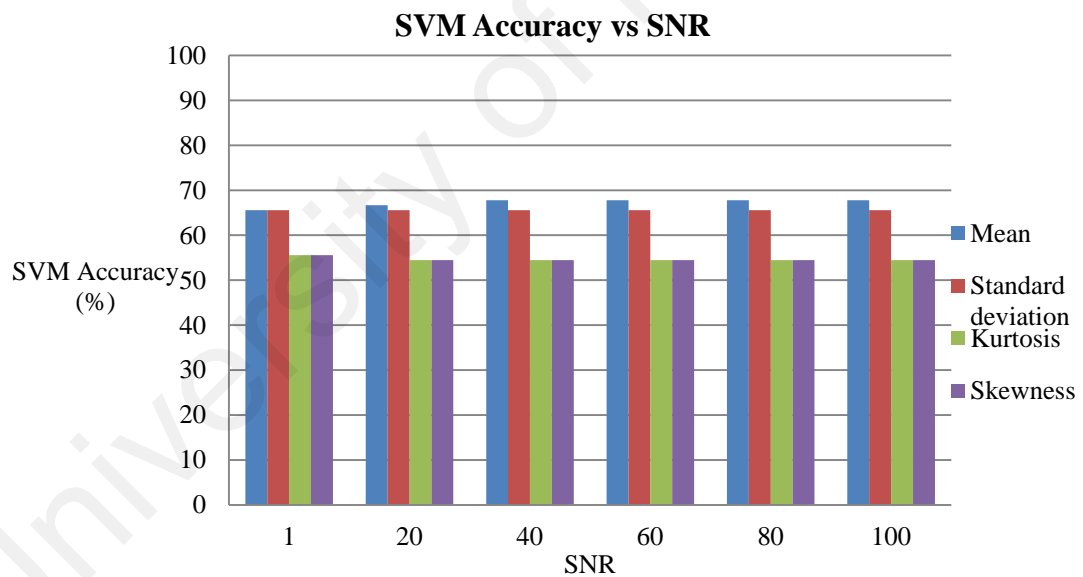


Figure 4.1: SVM accuracy average reading at different SNR for DFT signal

4.2.2 Statistical Features with Discrete Wavelet Transform

Table 4.6 shows SVM accuracy reading for mean feature with DWT signal at different SNR. For defect 1, the accuracy reading shows 100% from SNR = 1 until SNR = 100. For defect 2, the accuracy reading shows 66.6667% accuracy which was

maintained from SNR = 1 until SNR = 100. The accuracy reading shows zero values for SNR = 1 until SNR = 100 for defect 3 accuracy. The accuracy reading shows that there are no changes for all defect types from SNR = 1 until SNR = 100 for mean feature with DWT signal. Defect 1 and defect 2 have higher accuracy reading compared to defect 3. Hence, SVM can classify defect 1 and defect 2 correctly but cannot classify defect 3 correctly by using mean feature.

Table 4.6: SVM accuracy for DWT-mean

SVM ACCURACY (%)						
Defect Accuracy	Signal-to-noise-ratio (SNR)					
	1	20	40	60	80	100
1	100	100	100	100	100	100
2	66.6667	66.6667	66.6667	66.6667	66.6667	66.6667
3	0	0	0	0	0	0
Average	55.5556	55.5556	55.5556	55.5556	55.5556	55.5556

Table 4.7 shows SVM accuracy reading for standard deviation feature with DWT signal at different SNR for different defect types. For defect 1, the accuracy reading shows 100%, which was maintained from SNR = 1 until SNR = 100. For defect 2, the accuracy reading does not change from SNR = 1 until SNR = 100 which is 96.6667%. The accuracy reading shows zero values for SNR = 1 until SNR = 100 for defect 3. Defect 1 and defect 2 have higher accuracy reading compared to defect 3. Hence, SVM can classify defect 1 and defect 2 correctly but cannot classify defect 3 correctly by using standard deviation feature.

Table 4.7: SVM accuracy for DWT-standard deviation

SVM ACCURACY (%)						
Defect Accuracy	Signal-to-noise-ratio (SNR)					
	1	20	40	60	80	100
1	100	100	100	100	100	100
2	96.6667	96.6667	96.6667	96.6667	96.6667	96.6667
3	0	0	0	0	0	0
Average	65.5556	65.5556	65.5556	65.5556	65.5556	65.5556

Table 4.8 shows SVM accuracy reading for kurtosis feature with DWT signal at different SNR for different defect types. For defect 1, the accuracy reading shows 76.6667% for SNR = 1 until SNR = 40. Then, the reading of accuracy decreases from 76.6667% to 73.3333% for SNR = 60 until SNR = 100. For defect 2, the accuracy reading shows zero values for SNR = 1 until SNR = 100. The accuracy reading shows 100% for SNR = 1 until SNR = 100 for defect 3 type. Defect 3 has the highest accuracy reading which is 100% accuracy compared to defect 1 which is 76.6667% and 73.3333%. However, defect 2 has the lowest accuracy which is zero values of reading. SVM can classify defect 1 and defect 3 correctly but cannot classify defect 2 correctly by using kurtosis feature.

Table 4.8: SVM accuracy for DWT-kurtosis

SVM ACCURACY (%)						
Defect Accuracy	Signal-to-noise-ratio (SNR)					
	1	20	40	60	80	100
1	76.6667	76.6667	76.6667	73.3333	73.3333	73.3333
2	0	0	0	0	0	0
3	100	100	100	100	100	100
Average	58.8889	58.8889	58.8889	57.7778	57.7778	57.7778

Table 4.9 shows SVM accuracy reading for skewness feature with DWT signal at different SNR. For defect 1, the accuracy reading shows a perfect accuracy which is 100% for SNR = 1 until SNR = 100. For defect 2, the accuracy reading shows 80% value, which was maintained from SNR = 1 until SNR = 100. The accuracy reading shows zero values for SNR = 1 until SNR = 100 for defect 3 type. Defect 1 has the highest accuracy reading which is 100% accuracy compared to defect 2 which is 80% accuracy. However, defect 3 has the lowest accuracy which is zero. The accuracy reading shows that there are no changes for all defect types from SNR = 1 until SNR = 100 for skewness feature with DWT signal. SVM can classify defect 1 and defect 2 correctly but cannot classify defect 3 correctly by using skewness features.

Table 4.9: SVM accuracy for DWT-skewness

SVM ACCURACY (%)						
Defect	Signal-to-noise-ratio (SNR)					
Accuracy	1	20	40	60	80	100
1	100	100	100	100	100	100
2	80	80	80	80	80	80
3	0	0	0	0	0	0
Average	60	60	60	60	60	60

Table 4.10 shows SVM accuracy average reading of statistical features with DWT signal processing technique. For mean and standard deviation features, SVM accuracy average reading shows maintained values from SNR = 1 until SNR = 100 which is 55.5556% and 65.5556% respectively. For kurtosis feature, the average reading was maintained from SNR = 1 until SNR = 40 which is 58.8889% accuracy. Then, the average reading slightly decreases from 58.8889% to 57.7778% accuracy for SNR = 60. From SNR = 60 until SNR = 100, the average reading was maintained again which is 57.7778% accuracy. For skewness feature, SVM accuracy average reading does not change from SNR = 1 until SNR = 100 which is 60%. Figure 4.2 shows SVM accuracy average reading at different SNR for DWT signal processing technique. The figure shows that standard deviation has the highest accuracy average reading which is 65.5556% while mean has the lowest accuracy average reading which is 55.5556%.

Table 4.10: SVM accuracy average reading for DWT signal

SVM ACCURACY (%)						
Statistical Features	Signal-to-noise-ratio (SNR)					
	1	20	40	60	80	100
Mean	55.5556	55.5556	55.5556	55.5556	55.5556	55.5556
Standard deviation	65.5556	65.5556	65.5556	65.5556	65.5556	65.5556
Kurtosis	58.8889	58.8889	58.8889	57.7778	57.7778	57.7778
Skewness	60	60	60	60	60	60

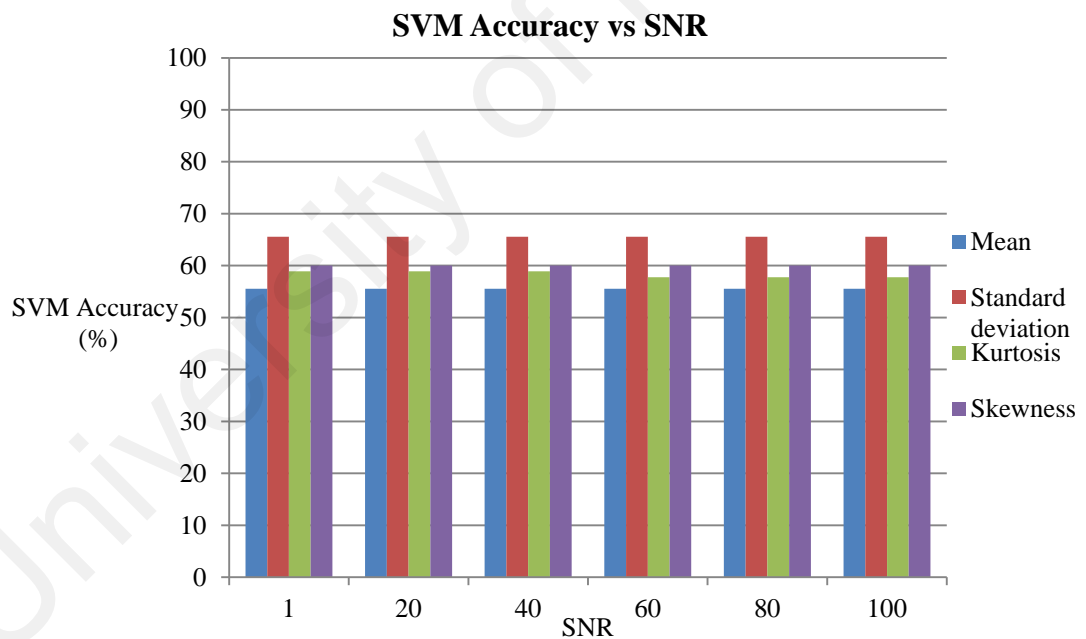


Figure 4.2: SVM accuracy average reading at different SNR for DWT signal

4.2.3 Statistical Features with Wavelet Packet Transform

Table 4.11 shows SVM accuracy reading for mean feature with WPT signal at different SNR. For defect 1, the accuracy reading shows 100% from SNR = 1 until SNR

= 100. For defect 2, the accuracy reading shows 66.6667% accuracy which was maintained from SNR = 1 until SNR = 100. The accuracy reading shows zero values for SNR = 1 until SNR = 100 for defect 3. Defect 1 and defect 2 have higher accuracy reading compared to defect 3. Hence, defect 1 and defect 2 can be classified correctly by SVM but cannot classify defect 3 correctly by using mean feature.

Table 4.11: SVM accuracy for WPT-mean

SVM ACCURACY (%)						
Defect Accuracy	Signal-to-noise-ratio (SNR)					
	1	20	40	60	80	100
1	100	100	100	100	100	100
2	66.6667	66.6667	66.6667	66.6667	66.6667	66.6667
3	0	0	0	0	0	0
Average	55.5556	55.5556	55.5556	55.5556	55.5556	55.5556

Table 4.12 shows SVM accuracy reading for standard deviation feature with WPT signal at different SNR for different defect types. For defect 1, the accuracy reading shows 100% rate which was maintained from SNR = 1 until SNR = 100. For defect 2, the accuracy reading also not change from SNR = 1 until SNR = 100 which was 96.6667%. The accuracy reading shows zero values for SNR = 1 until SNR = 100 for defect 3 accuracy. Defect 1 and defect 2 have higher accuracy reading compared to defect 3. The accuracy reading shows that there are no changes for all defect types from SNR = 1 until SNR = 100 for standard deviation feature with WPT signal. Hence, SVM can classify defect 1 and defect 2 correctly but cannot classify defect 3 correctly by using standard deviation feature.

Table 4.12: SVM accuracy for WPT-standard deviation

SVM ACCURACY (%)						
Defect Accuracy	Signal-to-noise-ratio (SNR)					
	1	20	40	60	80	100
1	100	100	100	100	100	100
2	96.6667	96.6667	96.6667	96.6667	96.6667	96.6667
3	0	0	0	0	0	0
Average	65.5556	65.5556	65.5556	65.5556	65.5556	65.5556

Table 4.13 shows SVM accuracy reading for kurtosis feature with WPT signal at different SNR for different defect types. For defect 1, the accuracy reading shows 76.6667% rate for SNR = 1 until SNR = 100. For defect 2, the accuracy reading shows zero values for SNR = 1 until SNR = 100. The accuracy reading shows 100% for SNR = 1 until SNR = 100 for defect 3 type. Defect 3 has the highest accuracy reading which is 100% accuracy compared to defect 1 which is 76.6667%. However, defect 2 has the lowest accuracy which is zero. SVM can classify defect 1 and defect 3 correctly but cannot classify defect 2 correctly by using kurtosis feature.

Table 4.13: SVM accuracy for WPT-kurtosis

SVM ACCURACY (%)						
Defect Accuracy	Signal-to-noise-ratio (SNR)					
	1	20	40	60	80	100
1	76.6667	76.6667	76.6667	76.6667	76.6667	76.6667
2	0	0	0	0	0	0
3	100	100	100	100	100	100
Average	58.8889	58.8889	58.8889	58.8889	58.8889	58.8889

Table 4.14 shows SVM accuracy reading for skewness feature with WPT signal at different SNR. For defect 1, the accuracy reading shows a perfect accuracy which is 100% for SNR = 1 until SNR = 100. For defect 2, the accuracy reading shows 80% value which was maintained for SNR = 1 until SNR = 100. The accuracy reading shows zero values for SNR = 1 until SNR = 100 for defect 3 type. Defect 1 has the highest accuracy reading which is 100% accuracy compared to defect 2 which is 80%. However, defect 3 has the lowest accuracy which is zero. SVM can classify defect 1 and defect 2 correctly but cannot classify defect 3 correctly by using skewness feature.

Table 4.14: SVM accuracy for WPT-skewness

SVM ACCURACY (%)						
Defect	Signal-to-noise-ratio (SNR)					
Accuracy	1	20	40	60	80	100
1	100	100	100	100	100	100
2	80	80	80	80	80	80
3	0	0	0	0	0	0
Average	60	60	60	60	60	60

Table 4.15 shows SVM accuracy average reading of statistical features with WPT signal processing technique. For mean and standard deviation features, SVM accuracy average reading shows maintained values from SNR = 1 until SNR = 100 which was 55.5556% and 65.5556% respectively. For kurtosis and skewness features, the average reading also does not change from SNR = 1 until SNR = 100 which was 58.8889% and 60% respectively. Hence, all accuracies were maintained for all the features from SNR = 1 until SNR = 100. Figure 4.3 shows SVM accuracy average reading at different SNR for WPT signal processing technique. The figure shows that standard deviation has the highest accuracy average reading among the others which is 65.5556%.

Table 4.15: SVM accuracy average reading for WPT signal

SVM ACCURACY (%)						
Statistical Features	Signal-to-noise-ratio (SNR)					
	1	20	40	60	80	100
Mean	55.5556	55.5556	55.5556	55.5556	55.5556	55.5556
Standard deviation	65.5556	65.5556	65.5556	65.5556	65.5556	65.5556
Kurtosis	58.8889	58.8889	58.8889	58.8889	58.8889	58.8889
Skewness	60	60	60	60	60	60

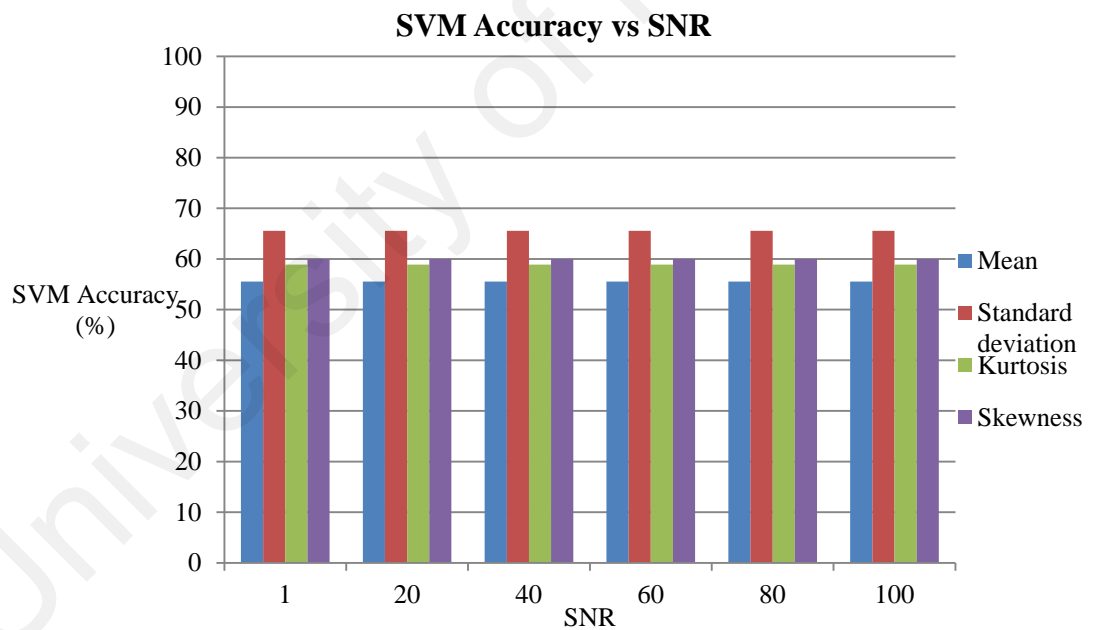


Figure 4.3: SVM accuracy average reading at different SNR for WPT signal

4.3 Classification Results by Artificial Neural Network

Before analysing the partial discharge (PD) classification, the raw data of PD signals need to be extracted first. Each PD signals was tested for a clean PD signals and by

adding noise. The signals were added with noise, resulting in signal-to-noise-ratio (SNR) of 1, 20, 40, 60 and 80dB. After the input signals was extracted by discrete Fourier transform (DFT), discrete wavelet transform (DWT) and wavelet packet transform (WPT), the signals was trained and classified by artificial neural network (ANN) to classify the defect types using MATLAB programming. The best results are shown by the highest accuracy value.

4.3.1 Statistical Features with Discrete Fourier Transform

Table 4.16 shows ANN accuracy reading for mean feature with DFT signal at different SNR. For defect 1 and defect 2, the accuracy reading shows 100% from SNR = 1 until SNR = 100. The accuracy reading shows 96.6667% value for SNR = 1, SNR = 40, SNR = 60 and SNR = 80 for defect 3 accuracy. For SNR = 20, the reading shows 90% accuracy and for SNR = 100, the reading shows 100% accuracy for defect 3. Defect 1 and defect 2 have the perfect accuracy reading. Hence, ANN can classify defect 1 and 2 correctly by using mean feature.

Table 4.16: ANN accuracy for DFT-mean

ANN ACCURACY (%)						
Defect Accuracy	Signal-to-noise-ratio (SNR)					
	1	20	40	60	80	100
1	100	100	100	100	100	100
2	100	100	100	100	100	100
3	96.6667	90	96.6667	96.6667	96.6667	100
Average	98.8889	96.6667	98.8889	98.8889	98.8889	100

Table 4.17 shows ANN accuracy reading for standard deviation feature with DFT signal at different SNR for different defect types. For defect 1 and defect 2, the accuracy reading shows 100% from SNR = 1 until SNR = 100. The accuracy reading shows 90% value of SNR = 1 for defect 3 accuracy. Then, the accuracy reading slowly decreases to 86.6667% for SNR = 20 until SNR = 80. For SNR = 100, the accuracy decreases again to 76.6667% for defect 3. Defect 1 and defect 2 have a perfect accuracy reading. Hence, ANN can classify defect 1 and 2 correctly by using standard deviation feature.

Table 4.17: ANN accuracy for DFT-standard deviation

ANN ACCURACY (%)						
Defect	Signal-to-noise-ratio (SNR)					
Accuracy	1	20	40	60	80	100
1	100	100	100	100	100	100
2	100	100	100	100	100	100
3	90	86.6667	86.6667	86.6667	86.6667	76.6667
Average	96.6667	95.5556	95.5556	95.5556	95.5556	92.2222

Table 4.18 shows ANN accuracy reading for kurtosis feature with DFT signal at different SNR. For defect 1, the accuracy reading shows 86.6667% rate for SNR = 1, SNR = 60 and SNR = 100. For SNR = 20, SNR = 40 and SNR = 80, the accuracy reading shows 83.3333% rate. For defect 2, the accuracy reading shows 100% value for SNR = 1. Then, the reading decreases to 96.6667% accuracy from SNR = 20 until SNR = 100. For defect 3, the accuracy has 100% value for SNR = 1 until SNR = 100. Defect 3 has a perfect accuracy reading. Hence, ANN can classify defect 3 correctly by using kurtosis feature.

Table 4.18: ANN accuracy for DFT-kurtosis

ANN ACCURACY (%)						
Defect Accuracy	Signal-to-noise-ratio (SNR)					
	1	20	40	60	80	100
1	86.6667	83.3333	83.3333	86.6667	83.3333	86.6667
2	100	96.6667	96.6667	96.6667	96.6667	96.6667
3	100	100	100	100	100	100
Average	95.5556	93.3333	93.3333	94.4444	93.3333	94.4444

Table 4.19 shows ANN accuracy reading for skewness feature with DFT signal at different SNR. For defect 1, the accuracy reading shows 80% for SNR = 1 and SNR = 100. For SNR = 20, the defect has the lowest accuracy value which is 73.3333%. For SNR = 40, the defect has the highest accuracy reading which is 86.6667%. For SNR = 60 and SNR = 80, both show the accuracy reading of 83.3333%. For defect 2, the accuracy reading shows 100% value for SNR = 1. Then, the value decreases to 96.6667% accuracy from SNR = 20 until SNR = 100. For defect 3, the accuracy is 100% for SNR = 1 until SNR = 40. However, the value decreases to 96.6667% accuracy for SNR = 60. Then, the reading of accuracy increases back to 100% value for SNR = 80 and SNR = 100.

Table 4.19: ANN accuracy for DFT-skewness

ANN ACCURACY (%)						
Defect Accuracy	Signal-to-noise-ratio (SNR)					
	1	20	40	60	80	100
1	80	73.3333	86.6667	83.3333	83.3333	80
2	100	96.6667	96.6667	96.6667	96.6667	96.6667
3	100	100	100	96.6667	100	100
Average	93.3333	90	94.4444	92.2222	93.3333	92.2222

Table 4.20 shows ANN accuracy average reading of statistical features for DFT signal processing technique. For mean feature, SNR = 100 has the highest accuracy reading which is 100% value followed by SNR = 1, SNR = 40, SNR = 60 and SNR = 80 which has the reading of 98.8889% accuracy. SNR = 20 has the lowest accuracy reading which is 96.6667% value. For standard deviation feature, SNR = 1 has the highest accuracy reading which is 96.6667% value followed by SNR = 20 until SNR = 80 which has the reading of 95.5556% accuracy. SNR = 100 has the lowest accuracy reading which is 92.2222% value. For kurtosis feature, SNR = 1 has the highest accuracy reading which is 95.5556% followed by SNR = 60 and SNR = 100 which have the reading of 94.4444% accuracy. SNR = 20, SNR = 40 and SNR = 80 have the lowest accuracy reading which is 93.3333% value. For skewness feature, SNR = 40 has the highest accuracy reading which is 94.4444% followed by SNR = 1 and SNR = 80 which has the reading of 93.3333% accuracy. Then, the value of accuracy decreases again to 92.2222% value for SNR = 60 and SNR = 100. SNR = 20 has the lowest accuracy reading which is 90% value. Figure 4.4 shows ANN accuracy average reading at

different SNR for DFT signal processing technique. The figure shows that mean has the highest accuracy average reading among the others which is 100%.

Table 4.20: ANN accuracy average reading for DFT signal

ANN ACCURACY (%)						
Statistical Features	Signal-to-noise-ratio (SNR)					
	1	20	40	60	80	100
Mean	98.8889	96.6667	98.8889	98.8889	98.8889	100
Standard deviation	96.6667	95.5556	95.5556	95.5556	95.5556	92.2222
Kurtosis	95.5556	93.3333	93.3333	94.4444	93.3333	94.4444
Skewness	93.3333	90	94.4444	92.2222	93.3333	92.2222

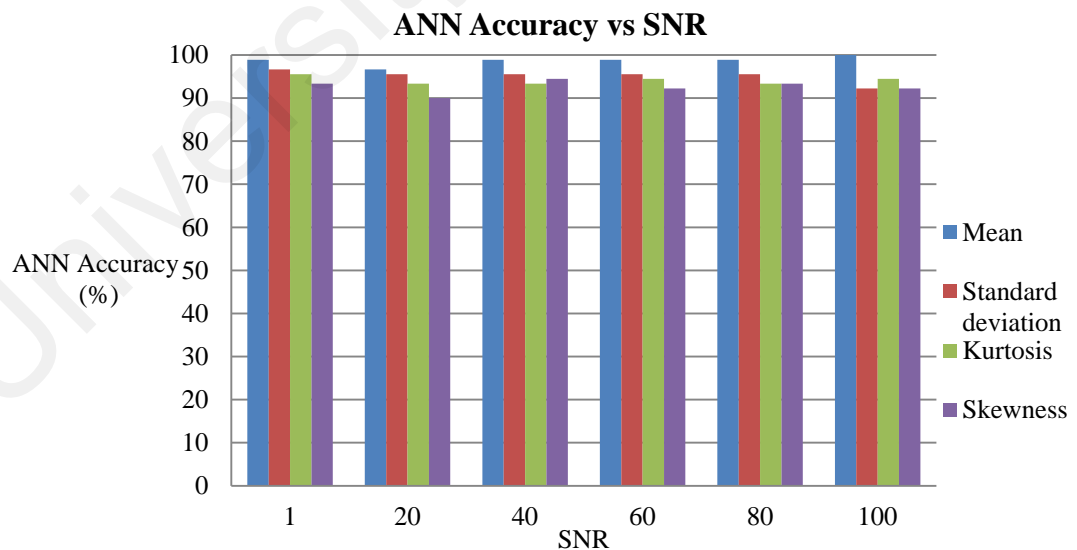


Figure 4.4: ANN accuracy average reading at different SNR for DFT signal

4.3.2 Statistical Features with Discrete Wavelet Transform

Table 4.21 shows ANN accuracy reading for mean feature with DWT signal at different SNR. For defect 1 and defect 2, the accuracy reading shows 100% from SNR = 1 until SNR = 100. The accuracy reading also shows a constant value which is 83.3333% value for SNR = 1 until SNR = 100 for defect 3. Defect 1 and defect 2 have a perfect accuracy reading. So, ANN can classify defect 1 and 2 correctly by using mean feature.

Table 4.21: ANN accuracy for DWT-mean

ANN ACCURACY (%)						
Defect Accuracy	Signal-to-noise-ratio (SNR)					
	1	20	40	60	80	100
1	100	100	100	100	100	100
2	100	100	100	100	100	100
3	83.3333	83.3333	83.3333	83.3333	83.3333	83.3333
Average	94.4444	94.4444	94.4444	94.4444	94.4444	94.4444

Table 4.22 shows ANN accuracy reading for standard deviation feature with DWT signal at different SNR for different defect types. For defect 1, the accuracy reading shows 100% from SNR = 1 until SNR = 100. For defect 2, the accuracy reading shows 100% value for SNR = 1, SNR = 20, SNR = 60, SNR = 80 and SNR = 100. SNR = 40 shows the lowest accuracy reading which is 96.6667%. For SNR = 1, SNR = 20, SNR = 60 and SNR = 100, defect 3 has the highest accuracy reading which is 96.6667% value. For SNR = 40 and SNR = 80, defect 3 has the lowest accuracy reading which is 86.6667% for both SNR. Defect 1 has a perfect accuracy reading compared to defect 2

and defect 3. Hence, ANN can classify defect 1 correctly by using standard deviation feature.

Table 4.22: ANN accuracy for DWT-standard deviation

ANN ACCURACY (%)						
Defect Accuracy	Signal-to-noise-ratio (SNR)					
	1	20	40	60	80	100
1	100	100	100	100	100	100
2	100	100	96.6667	100	100	100
3	96.6667	96.6667	86.6667	96.6667	86.6667	96.6667
Average	98.8889	98.8889	94.4444	98.8889	95.5556	98.8889

Table 4.23 shows ANN accuracy reading for kurtosis feature with DWT signal at different SNR. For defect 1, the accuracy reading shows 76.6667% for SNR = 60 which was the highest value of accuracy reading. Then, the value decreases to 73.3333% of accuracy for SNR = 20, SNR = 40, SNR = 80 and SNR = 100 followed by SNR = 1 which is 56.6667%. For defect 2, the accuracy reading shows 100% value for SNR = 1, SNR = 20, SNR = 40, SNR = 80 and SNR = 100. However, the reading decreases to 96.6667% accuracy for SNR = 60. For defect 3, the accuracy has a constant value of accuracy which is 96.6667% value for SNR = 1 until SNR = 100.

Table 4.23: ANN accuracy for DWT-kurtosis

ANN ACCURACY (%)						
Defect Accuracy	Signal-to-noise-ratio (SNR)					
	1	20	40	60	80	100
1	56.6667	73.3333	73.3333	76.6667	73.3333	73.3333
2	100	100	100	96.6667	100	100
3	96.6667	96.6667	96.6667	96.6667	96.6667	96.6667
Average	84.4444	90	90	90	90	90

Table 4.24 shows ANN accuracy reading for skewness feature with DWT signal at different SNR. For defect 1, the accuracy reading shows 93.3333% for SNR = 20 which is the highest value of accuracy reading. However, the value decreases to 90% of accuracy for SNR = 1 and SNR = 80 followed by SNR = 60 and SNR = 100 which is 86.6667%. SNR = 40 has the lowest accuracy reading for defect 1 which is 83.3333% value. For defect 2, the accuracy reading shows 100% value for SNR = 1, SNR = 40, SNR = 60, SNR = 80 and SNR = 100. Then, the reading decreases to 96.6667% accuracy for SNR = 20. For defect 3, the accuracy has a perfect accuracy which is 100% value for SNR = 1 until SNR = 100. Defect 3 has a perfect accuracy reading compared to defect 1 and defect 2. Hence, ANN can classify defect 3 correctly by using skewness feature.

Table 4.24: ANN accuracy for DWT-skewness

ANN ACCURACY (%)						
Defect	Signal-to-noise-ratio (SNR)					
Accuracy	1	20	40	60	80	100
1	90	93.3333	83.3333	86.6667	90	86.6667
2	100	96.6667	100	100	100	100
3	100	100	100	100	100	100
Average	96.6667	96.6667	94.4444	95.5556	96.6667	95.5556

Table 4.25 shows ANN accuracy average reading of statistical features for DWT signal processing technique. For mean feature, the accuracy reading did not change from SNR = 1 until SNR = 100 which is 94.4444% of value. For standard deviation feature, SNR = 1, SNR = 20, SNR = 60 and SNR = 100 have the highest accuracy reading which is 98.8889% value followed by SNR = 80 which has the reading of 95.5556% accuracy. SNR = 40 has the lowest accuracy reading which is 94.4444% value. For kurtosis feature, SNR = 1 has the lowest accuracy reading which is 84.4444%. SNR = 20, SNR = 40, SNR = 60, SNR = 80 and SNR = 100 have the highest accuracy reading which is 90% value. For skewness feature, SNR = 1, SNR = 20 and SNR = 80 have the highest accuracy reading which is 96.6667% value followed by SNR = 60 and SNR = 100 which have the reading of 95.5556% accuracy. SNR = 40 has the lowest accuracy reading which is 94.4444% value. Figure 4.5 shows ANN accuracy average reading at different SNR for DWT signal processing technique. The figure shows that standard deviation has the highest accuracy average reading among the others which is 98.8889% while kurtosis has the lowest accuracy reading.

Table 4.25: ANN accuracy average reading for DWT signal

ANN ACCURACY (%)						
Statistical Features	Signal-to-noise-ratio (SNR)					
	1	20	40	60	80	100
Mean	94.4444	94.4444	94.4444	94.4444	94.4444	94.4444
Standard deviation	98.8889	98.8889	94.4444	98.8889	95.5556	98.8889
Kurtosis	84.4444	90	90	90	90	90
Skewness	96.6667	96.6667	94.4444	95.5556	96.6667	95.5556

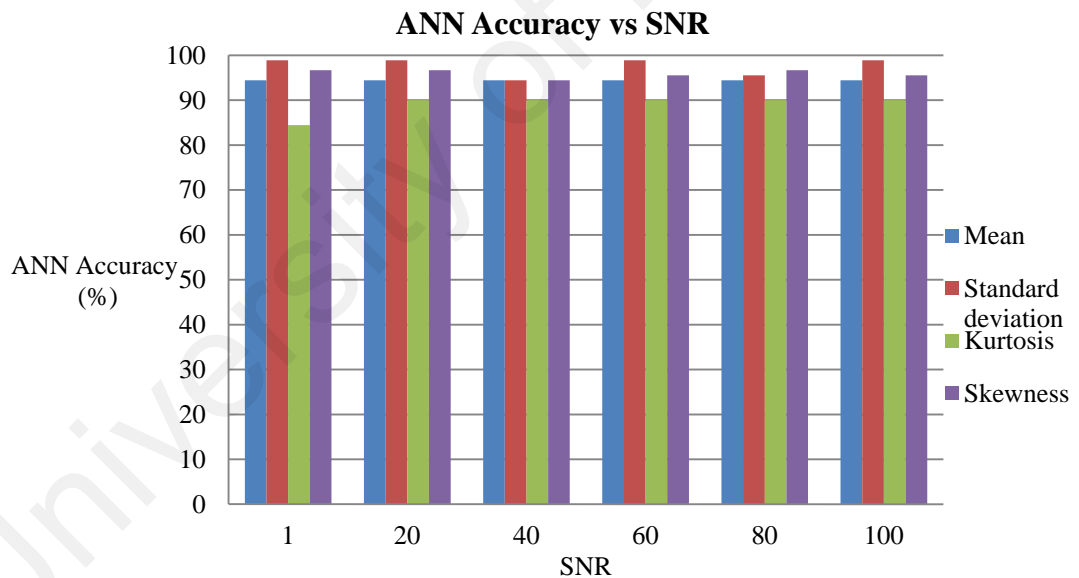


Figure 4.5: ANN accuracy average reading at different SNR for DWT signal

4.3.3 Statistical Features with Wavelet Packet Transform

Table 4.26 shows ANN accuracy reading for mean feature with WPT signal at different SNR. For defect 1 and defect 2, the accuracy reading shows 100% from SNR = 1 until SNR = 100. The accuracy reading shows a highest value which is 83.3333%

value for SNR = 1, SNR = 20, SNR = 60, SNR = 80 and SNR = 100 for defect 3. The value for SNR = 40 shows the lowest of accuracy reading which is 80%. Defect 1 and defect 2 have a perfect accuracy reading. Hence, ANN can classify defect 1 and 2 correctly by using mean feature.

Table 4.26: ANN accuracy for WPT-mean

ANN ACCURACY (%)						
Defect	Signal-to-noise-ratio (SNR)					
Accuracy	1	20	40	60	80	100
1	100	100	100	100	100	100
2	100	100	100	100	100	100
3	83.3333	83.3333	80	83.3333	83.3333	83.3333
Average	94.4444	94.4444	93.3333	94.4444	94.4444	94.4444

Table 4.27 shows ANN accuracy reading for standard deviation feature with WPT signal at different SNR for different defect types. For defect 1 and defect 2, the accuracy reading shows 100% from SNR = 1 until SNR = 100. For defect 3, SNR = 1 and SNR = 80 show the lowest accuracy reading which is 86.6667% rate followed by SNR = 20 which has 93.3333% accuracy reading. SNR = 40, SNR = 60 and SNR = 100 have the highest accuracy reading which is 96.6667%. Defect 1 and defect 2 have a perfect accuracy reading. Hence, ANN can classify defect 1 and 2 correctly by using standard deviation feature.

Table 4.27: ANN accuracy for WPT-standard deviation

ANN ACCURACY (%)						
Defect	Signal-to-noise-ratio (SNR)					
Accuracy	1	20	40	60	80	100
1	100	100	100	100	100	100
2	100	100	100	100	100	100
3	86.6667	93.3333	96.6667	96.6667	86.6667	96.6667
Average	95.5556	97.7778	98.8889	98.8889	95.5556	98.8889

Table 4.28 shows ANN accuracy reading for kurtosis feature with WPT signal at different SNR. For defect 1, the accuracy reading shows 76.6667% for SNR = 40 and SNR = 60 which was the highest value of accuracy reading. Then, the value was decreased to 73.3333% of accuracy for SNR = 20, SNR = 80 and SNR = 100 followed by SNR = 1 which is 63.3333%. For defect 2, the accuracy reading shows 100% value for SNR = 20 and SNR = 100. Then, the reading decreases to 96.6667% accuracy for SNR = 40, SNR = 60 and SNR = 80. SNR = 1 has the lowest accuracy reading which is 93.3333%. For defect 3, the accuracy has a highest of accuracy reading which is 100% value for SNR = 1, SNR = 20 and SNR = 80. SNR = 40, SNR = 60 and SNR = 100 have the lowest values of accuracy which is 96.6667%.

Table 4.28: ANN accuracy for WPT-kurtosis

ANN ACCURACY (%)						
Defect Accuracy	Signal-to-noise-ratio (SNR)					
	1	20	40	60	80	100
1	63.3333	73.3333	76.6667	76.6667	73.3333	73.3333
2	93.3333	100	96.6667	96.6667	96.6667	100
3	100	100	96.6667	96.6667	100	96.6667
Average	85.5556	91.1111	90	90	90	90

Table 4.29 shows ANN accuracy reading for skewness feature with WPT signal at different SNR. For defect 1, the accuracy reading shows 93.3333% rate for SNR = 40 which has the highest value of accuracy reading. Then, the value decreases to 90% of accuracy for SNR = 20 followed by SNR = 60 and SNR = 80 which is 86.6667%. SNR = 1 and SNR = 100 have the lowest accuracy reading for defect 1 which is 83.3333% value. For defect 2, the accuracy reading shows 100% value for SNR = 1, SNR = 20, SNR = 60, SNR = 80 and SNR = 100. Then, the reading decreases to 96.6667% accuracy for SNR = 40. For defect 3, the accuracy has a perfect accuracy which is 100% for SNR = 1 until SNR = 100. Defect 3 has a perfect accuracy reading. Hence, ANN can classify defect 3 correctly by using skewness feature.

Table 4.29: ANN accuracy for WPT-skewness

ANN ACCURACY (%)						
Defect	Signal-to-noise-ratio (SNR)					
Accuracy	1	20	40	60	80	100
1	83.3333	90	93.3333	86.6667	86.6667	83.3333
2	100	100	96.6667	100	100	100
3	100	100	100	100	100	100
Average	94.4444	96.6667	96.6667	95.5556	95.5556	94.4444

Table 4.30 shows ANN accuracy average reading of statistical features for WPT signal processing technique. For mean feature, the accuracy reading was highest for SNR = 1, SNR = 20, SNR = 60, SNR = 80 and SNR = 100 which is 94.4444% of value. SNR = 40 has the lowest accuracy reading which is 93.3333%. For standard deviation feature, SNR = 40, SNR = 60 and SNR = 100 have the highest accuracy reading which is 98.8889% value followed by SNR = 20 which has the reading of 97.7778% accuracy. SNR = 1 and SNR = 80 have the lowest accuracy reading which is 95.5556% value. For kurtosis feature, SNR = 1 has the lowest accuracy reading which is 85.5556% followed by SNR = 40, SNR = 60 and SNR = 80 and SNR = 100 which have 90% of accuracy reading. SNR = 20 has the highest accuracy reading which is 91.1111% value. For skewness feature, SNR = 20 and SNR = 40 have the highest accuracy reading which is 96.6667% value followed by SNR = 60 and SNR = 80 which have the reading of 95.5556% accuracy. SNR = 1 and SNR = 100 have the lowest accuracy reading which is 94.4444% value. Figure 4.5 shows ANN accuracy average reading at different SNR for WPT signal processing technique. The figure shows that standard deviation has the

highest accuracy average reading which is 98.8889% while kurtosis shows the lowest accuracy average reading.

Table 4.30: ANN accuracy average reading for WPT signal

ANN ACCURACY (%)						
Statistical Features	Signal-to-noise-ratio (SNR)					
	1	20	40	60	80	100
Mean	94.4444	94.4444	93.3333	94.4444	94.4444	94.4444
Standard deviation	95.5556	97.7778	98.8889	98.8889	95.5556	98.8889
Kurtosis	85.5556	91.1111	90	90	90	90
Skewness	94.4444	96.6667	96.6667	95.5556	95.5556	94.4444

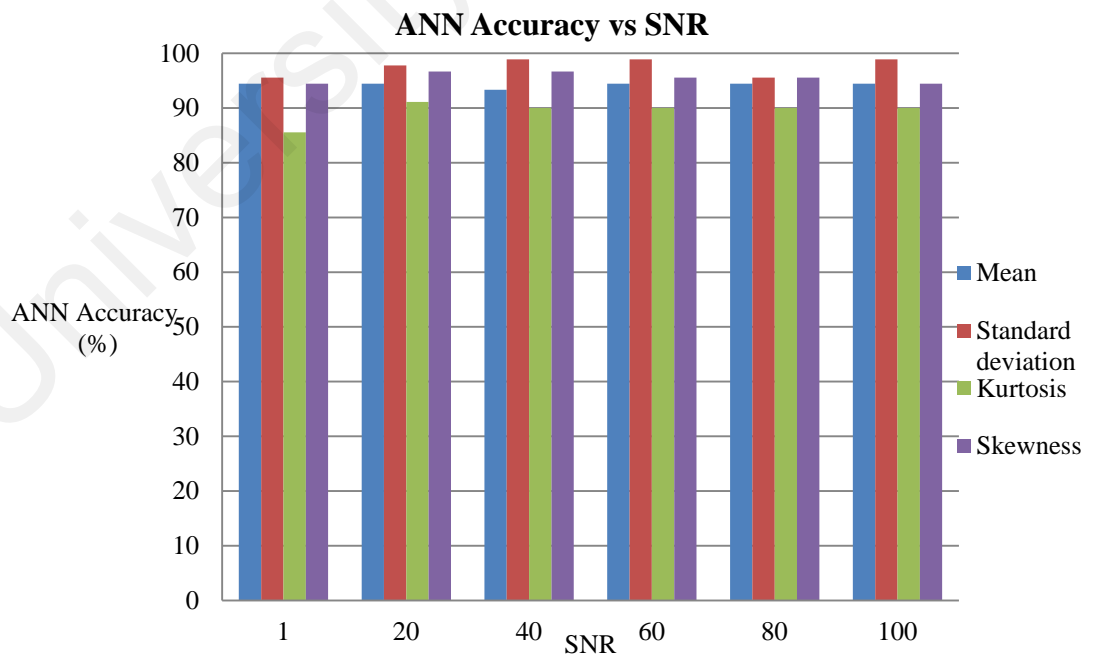


Figure 4.6: ANN accuracy average reading at different SNR for WPT signal

4.3.4 PCA Feature with Discrete Fourier Transform

Table 4.31 shows ANN accuracy reading for PCA feature with DFT signal processing technique at different SNR for different defect types. For defect 1, the highest accuracy is 43.3333% which is for SNR = 60, followed by 16.6667% accuracy value for SNR = 1. SNR = 20, SNR = 40, SNR = 80 and SNR = 100 have a zero accuracy reading. For defect 2, the accuracy reading shows 100% for SNR = 40. Both of SNR = 20 and SNR = 100 have accuracy reading of 96.6667% followed by SNR = 80 which is 90% accuracy reading. Both SNR = 1 and SNR = 60 have the lowest accuracy reading which are 73.3333% and 83.3333% respectively. For defect 3, SNR = 1, SNR = 20 and SNR = 80 show the highest accuracy reading which is 10% rate followed by SNR = 100 which has 3.3333% accuracy reading. Both of SNR = 40 and SNR = 60 have zero accuracy reading. Defect 2 has the highest accuracy reading compared to defect 1 and defect 3.

Table 4.31: ANN accuracy for DFT-PCA

ANN ACCURACY (%)						
Defect Accuracy	Signal-to-noise-ratio (SNR)					
	1	20	40	60	80	100
1	16.6667	0	0	43.3333	0	0
2	73.3333	96.6667	100	83.3333	90	96.6667
3	10	10	0	0	10	3.3333
Average	33.3333	35.5556	33.3333	42.2222	33.3333	33.3333

4.3.5 PCA Feature with Discrete Wavelet Transform

Table 4.32 shows ANN accuracy reading for PCA feature with DWT signal processing technique at different SNR. For defect 1, the highest accuracy is 33.3333% which is for SNR = 20, followed by 30% accuracy value for SNR = 60. SNR = 1, SNR = 40, SNR = 80 and SNR = 100 have zero accuracy. For defect 2, SNR = 100 shows the highest accuracy reading which is 80% followed by SNR = 20 which has 70% accuracy reading. SNR = 1, SNR = 40 and SNR = 60 have 63.3333%, 66.6667% and 56.6667% accuracies reading accordingly. SNR = 80 has the lowest accuracy reading which is 23.3333%. For defect 3, SNR = 80 shows the highest accuracy reading which is 86.6667% followed by SNR = 40, SNR = 1 and SNR = 100 which have 36.6667%, 33.3333% and 26.6667% accuracy reading respectively. SNR = 60 and SNR = 20 have the lowest accuracy reading which is 13.3333% and zero value of accuracy reading respectively.

Table 4.32: ANN accuracy for DWT-PCA

ANN ACCURACY (%)						
Defect Accuracy	Signal-to-noise-ratio (SNR)					
	1	20	40	60	80	100
1	0	33.3333	0	30	0	0
2	63.3333	70	66.6667	56.6667	23.3333	80
3	33.3333	0	36.6667	13.3333	86.6667	26.6667
Average	32.2222	34.4444	34.4444	33.3333	36.6667	35.5556

4.3.6 PCA Feature with Wavelet Packet Transform

Table 4.33 shows ANN accuracy reading for PCA feature with WPT signal processing technique at different SNR for different defect type. For defect 1, the highest accuracy is 13.3333% which is for SNR = 60. Both SNR = 20 and SNR = 100 have the same values of accuracy reading which was 6.6667%. This type of defect shows that SNR = 1, SNR = 40 and SNR = 80 have zero accuracy. For defect 2, SNR = 1 and SNR = 100 show the highest accuracy reading which is 93.3333% followed by SNR = 60 which has 86.6667% accuracy reading. Both SNR = 20 and SNR = 80 have 76.6667% and 60% values of accuracy reading. SNR = 40 has the lowest accuracy reading which is 33.3333%. For defect 3, SNR = 40 shows the highest accuracy reading which is 70% followed by SNR = 80, SNR = 1 and SNR = 20 which have 56.6667%, 10% and 3.3333% accuracy reading respectively. Both of SNR = 60 and SNR = 100 have zero accuracy reading. Defect 2 has higher accuracy reading compared to defect 1 and defect 3.

Table 4.33: ANN accuracy for WPT-PCA

ANN ACCURACY (%)						
Defect Accuracy	Signal-to-noise-ratio (SNR)					
	1	20	40	60	80	100
1	0	6.6667	0	13.3333	0	6.6667
2	93.3333	76.6667	33.3333	86.6667	60	93.3333
3	10	3.3333	70	0	56.6667	0
Average	34.4444	28.8889	34.4444	33.3333	38.8889	33.3333

Table 4.34 shows ANN accuracy average reading of PCA feature with DFT, DWT and WPT signal processing techniques. For DFT signal, the accuracy reading is the highest for SNR = 60 which is 42.2222% followed by SNR = 20 which has 35.5556% value of accuracy reading. SNR = 1, SNR = 40, SNR = 80 and SNR = 100 have the same values of accuracy reading which is 33.3333% rate. For DWT signal, SNR = 80 has the highest accuracy reading which is 36.6667% value followed by SNR = 100 which has the reading of 35.5556% accuracy. SNR = 20 and SNR = 40 have the same values of accuracy reading which is 34.4444%. SNR = 1 and SNR = 60 have the lowest accuracy reading which are 32.2222% and 33.3333%. For WPT, SNR = 80 has the highest accuracy reading which is 38.8889% value. For SNR = 1, SNR = 40 and SNR = 60, SNR = 100, they have the same values of accuracy reading which are 34.44445 and 33.3333% respectively. SNR = 20 has the lowest accuracy reading which is 28.8889%. Figure 4.7 shows ANN accuracy average reading at different SNR for PCA feature. The figure shows that DFT signal has the highest accuracy average reading among the others which is 42.2222%.

Table 4.34: ANN accuracy average reading for PCA feature

ANN ACCURACY (%)						
Signal Processing	Signal-to-noise-ratio (SNR)					
	1	20	40	60	80	100
DFT	33.3333	35.5556	33.3333	42.2222	33.3333	33.3333
DWT	32.2222	34.4444	34.4444	33.3333	36.6667	35.5556
WPT	34.4444	28.8889	34.4444	33.3333	38.8889	33.3333

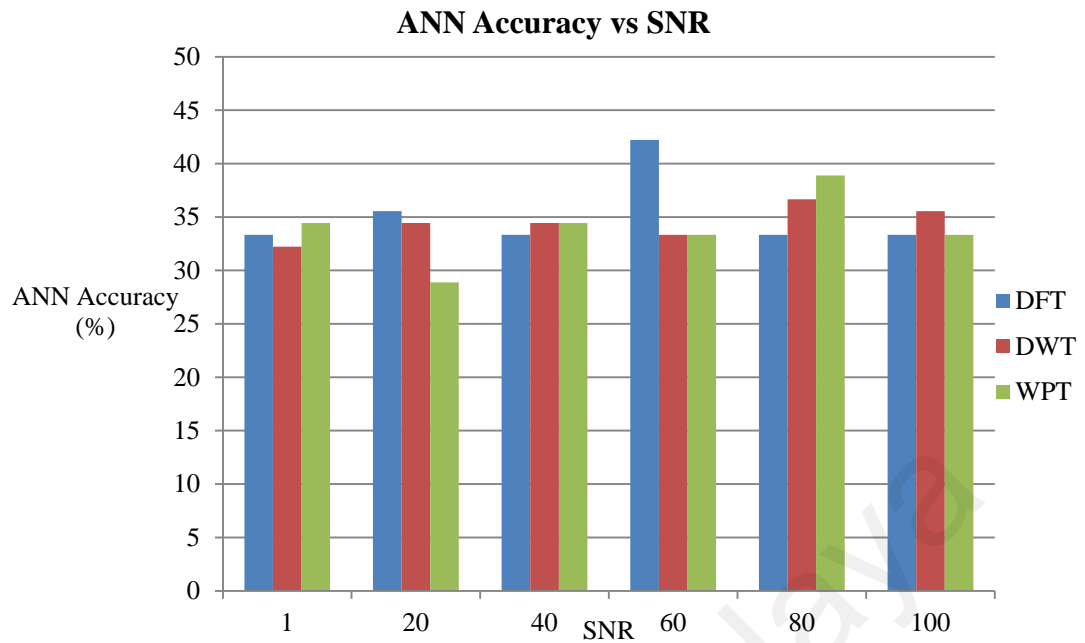


Figure 4.7: ANN accuracy average reading at different SNR for PCA feature

4.4 Overall Best Results of SVM and ANN Classification

This section discussed the overall best results computed by the features extraction methods with signal processing techniques. These features were classified by the SVM and ANN classifiers. The best results are shown by the highest overall accuracy.

4.4.1 Statistical Features of SVM and ANN Classifiers

Table 4.35 shows the best results of SVM and ANN classifiers for statistical features with signal processing techniques. For SVM classifier, mean feature with DFT signal processing technique shows the highest accuracy of classification defect types which is 67.7778%. For standard deviation feature with DWT and WPT signals, they have the same accuracy reading of classification which is 65.5556%. For ANN classifier, mean feature with DFT signal processing technique also shows the highest accuracy of classification defect types which is 100% accuracy. For standard deviation feature with DWT and WPT signals, they have the same accuracy reading of classification which is

98.8889% rate. Figure 4.8 shows overall accuracy at different signals for statistical features. The figure shows that mean feature with DFT signal by using ANN classifier has the highest accuracy which is 100% accuracy compared to SVM classifier.

Table 4.35: Best results of statistical features

Signal Processing Techniques	Statistical Features		Classifiers Accuracy (%)	
	Mean	Standard deviation	SVM	ANN
DFT	√		67.7778	100
DWT		√	65.5556	98.8889
WPT		√	65.5556	98.8889

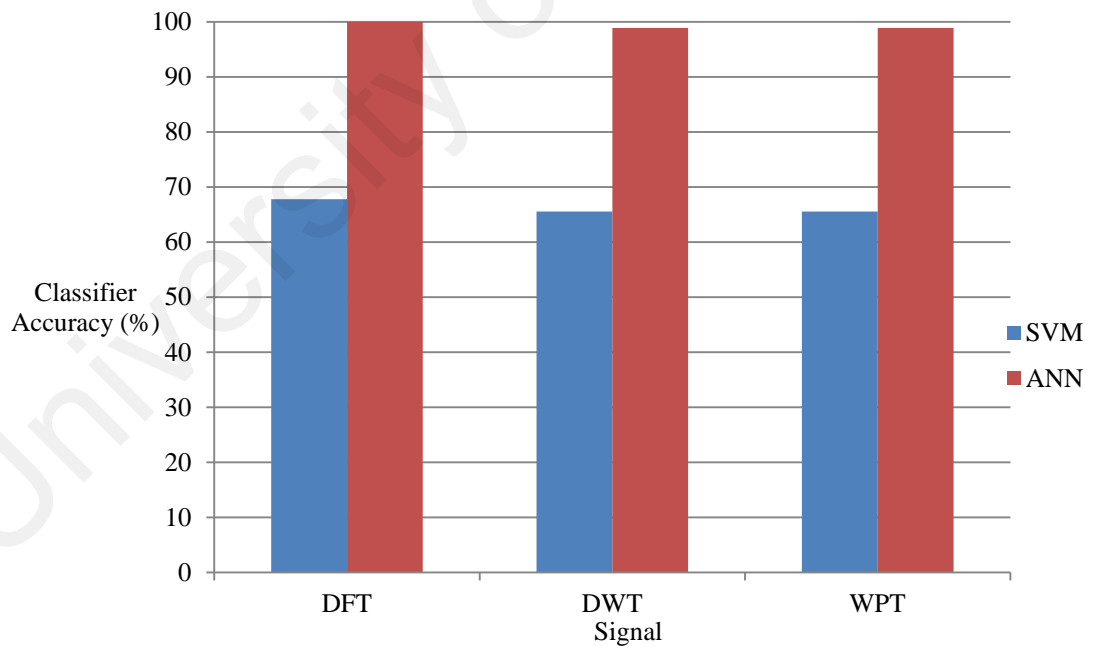


Figure 4.8: Overall accuracy at different signal for statistical features

4.4.2 PCA Feature of ANN Classifier

Table 4.36 shows the best results of ANN classifier for PCA feature. DFT signal processing technique shows the highest accuracy of classification defect types which is 42.2222% followed by WPT signal which shows 38.8889% of accuracy reading. DWT signal shows the lowest accuracy reading which is 36.6667% rate. Figure 4.9 shows an overall accuracy at different signals for PCA features. The figure shows that PCA feature with DFT signal by using ANN classifier has the highest accuracy reading which is 42.2222% accuracy.

Table 4.36: Best results of PCA feature

Signal Processing Techniques	ANN Accuracy (%)
DFT	42.2222
DWT	36.6667
WPT	38.8889

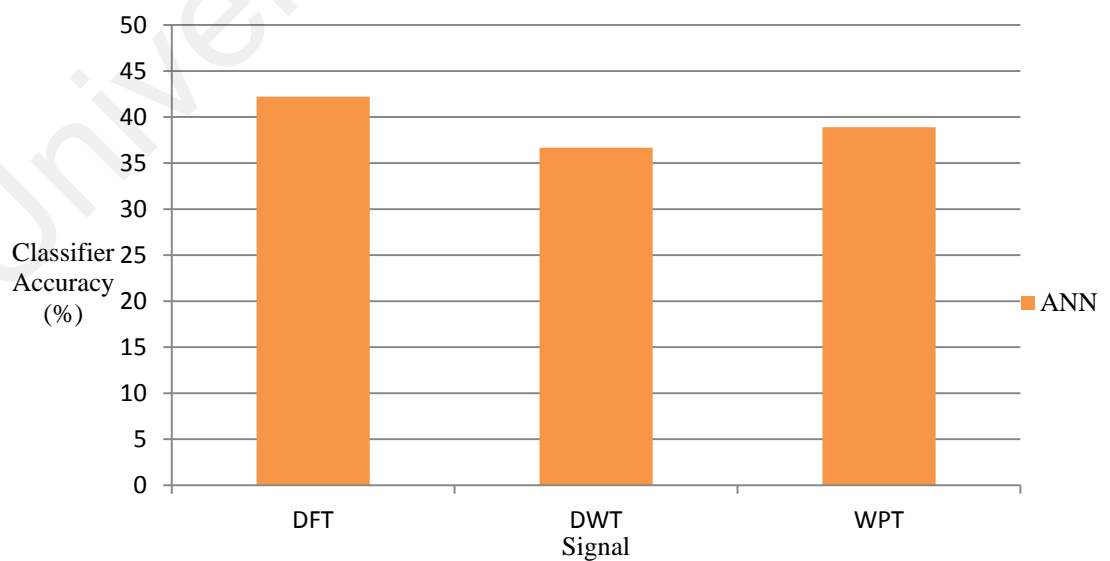


Figure 4.9: Overall accuracy at different signal for PCA feature

4.5 Comparison with Previous Works

The best results with highest accuracy values that have been obtained from ANN classifier were compared with some of the related previous works. The best result that has been obtained from this work is statistical features with DFT signal processing technique by using ANN classifier. Table 4.37 shows a comparison of the classification accuracy of this work with the past works. From the table, it can be seen that the results obtained from this work are in reasonable agreement with the previous works. Therefore, the statistical features as an input feature and trained using ANN classifier can be considered as a suitable method to classify the defect types in XLPE cable joints.

Table 4.37: Comparison with the past works

Proposed Work	ANN Classification Accuracy
Classification of Defect Types in Cross-Linked Polyethylene (XLPE) Cable Joints - Statistical features with DFT signal processing technique using ANN classifier	100%
Existing Works	ANN Classification Accuracy
Abubakar Mas'ud, Stewart et al. 2014 - Artificial defects created in laboratory - Statistical features	95%

<p>Shurrab, El-Haag et al. 2013</p> <ul style="list-style-type: none"> - Silicon rubber surface as test subject - Statistical and spectral features 	<p>96%</p>
<p>Boczar, Borucki et al. 2009</p> <ul style="list-style-type: none"> - Paper oil insulation as test subject - Fourier transform and power spectrum density 	<p>90%</p>
<p>Li, Sun et al. 2006</p> <ul style="list-style-type: none"> -Artificial defect model tests - Statistical features - Fractal features 	<p>Statistical features – 88.44%</p> <p>Fractal features – 84.26%</p>
<p>Karthikeyan, Gopal et al. 2005</p> <ul style="list-style-type: none"> - Perspex material as a test subject - Statistical features 	<p>100%</p>

CHAPTER 5: CONCLUSIONS AND RECOMMENDATIONS

5.1 Conclusions

In this work, classification of defect types in cross-linked polyethylene (XLPE) cable joints using partial discharge (PD) measurement has been successfully carried out. From the PD signals obtained, features extraction were successfully performed using statistical features and principle component analysis (PCA) with discrete Fourier transform (DFT), discrete wavelet transform (DWT) and wavelet packet transform (WPT) signal processing techniques. These features were successfully used as the input data for support vector machine (SVM) and artificial neural network (ANN) to classify the defect types in XLPE cable joints. The accuracy results of the proposed methods were compared with each other to identify the best method, which yields the highest accuracy. From the results obtained, it was found that input feature of mean with DFT signal processing technique and classified using ANN classifier managed to classify the defect types with the highest accuracy. Comparison with previous works also shows that the results obtained from this work are acceptable. Therefore, the input feature using mean with DFT signal processing technique and trained with ANN classifier can be considered a suitable method as a classification tool to classify the defect types in XLPE cable joints, which can facilitate the maintenance and diagnosis of HV equipment.

5.2 Recommendations for Future Works

Future works that can be performed from this research work are as follows:

1. Capture partial discharge (PD) signals from different high voltage equipment in the experimental setup
2. Use other input features from signal processing techniques
3. Classify using other artificial intelligence methods

REFERENCES

- Ab Aziz, N. F., et al. (2007). Analysis of partial discharge measurement data using a support vector machine. Research and Development, 2007. SCOReD 2007. 5th Student Conference on, IEEE.
- Abubakar Mas'ud, A., et al. (2014). "Application of an ensemble neural network for classifying partial discharge patterns." Electric Power Systems Research **110**: 154-162.
- Al-geelani, N. A., et al. (2015). "A review on hybrid wavelet regrouping particle swarm optimization neural networks for characterization of partial discharge acoustic signals." Renewable and Sustainable Energy Reviews **45**: 20-35.
- Angrisani, L., et al. (2000). "Analysis of ultrawide-band detected partial discharges by means of a multiresolution digital signal-processing method." Measurement **27**(3): 207-221.
- Babnik, T., et al. (2007). "Data mining on a transformer partial discharge data using the self-organizing map." IEEE Transactions on Dielectrics and Electrical Insulation **14**(2): 444-452.
- Bartnikas, R. (2002). "Partial discharges. Their mechanism, detection and measurement." IEEE Transactions on Dielectrics and Electrical Insulation **9**(5): 763-808.
- Boczar, T., et al. (2009). "Application possibilities of artificial neural networks for recognizing partial discharges measured by the acoustic emission method." IEEE Transactions on Dielectrics and Electrical Insulation **16**(1): 214-223.
- Boyle, B. H. (2011). Support Vector Machines: Data Analysis, Machine Learning and Applications, Nova Science Publishers, Inc.
- Chan, Y. (2012). Wavelet basics, Springer Science & Business Media.
- Chen, H.-C., et al. (2012). "A novel extension neural network based partial discharge pattern recognition method for high-voltage power apparatus." Expert Systems with Applications **39**(3): 3423-3431.
- Chen, M., et al. (2014). "Partial discharge detection by RF coil in 161 kV power transformer." IEEE Transactions on Dielectrics and Electrical Insulation **21**(3): 1405-1414.

Chen, X., et al. (2014). "Nonlinear time series analysis of partial discharges in electrical trees of XLPE cable insulation samples." IEEE Transactions on Dielectrics and Electrical Insulation **21**(4): 1455-1461.

Cho, Y.-S., et al. (1998). "Electrical tree initiation mechanism of artificial defects filled XLPE." Materials chemistry and physics **56**(1): 87-90.

Corte-Valiente, A. d., et al. (2017). "An Artificial Neural Network for Analyzing Overall Uniformity in Outdoor Lighting Systems." Energies **10**(2): 175.

Cosgrave, J., et al. (1993). "Acoustic monitoring of partial discharges in gas insulated substations using optical sensors." IEE Proceedings A (Science, Measurement and Technology) **140**(5): 369-374.

de Oliveira Mota, H., et al. (2011). "Partial discharge signal denoising with spatially adaptive wavelet thresholding and support vector machines." Electric Power Systems Research **81**(2): 644-659.

Devore, J. L. (2011). Probability and Statistics for Engineering and the Sciences, Cengage learning.

Edin, H. (2001). Partial discharges studied with variable frequency of the applied voltage, KTH.

Evagorou, D., et al. (2010). "Feature extraction of partial discharge signals using the wavelet packet transform and classification with a probabilistic neural network." IET science, measurement & technology **4**(3): 177-192.

Furstenau, N., et al. (1997). "Extrinsic Fabry-Perot interferometer vibration and acoustic sensor systems for airport ground traffic monitoring." IEE Proceedings-Optoelectronics **144**(3): 134-144.

Gençoğlu, M. and M. Cebeci (2009). "Investigation of pollution flashover on high voltage insulators using artificial neural network." Expert Systems with Applications **36**(4): 7338-7345.

Ghaffarian Niasar, M. (2012). Partial discharge signatures of defects in insulation systems consisting of oil and oil-impregnated paper, KTH Royal Institute of Technology.

Gonzalez, R. C. and R. E. Woods (2002). Digital image processing, Prentice hall New Jersey.

Greene, J. A., et al. (1995). "Optical fiber sensing technique for impact detection and location in composites and metal specimens." Smart Materials and Structures **4**(2): 93.

Gu, F.-C., et al. (2012). "Partial discharge pattern recognition of power cable joints using extension method with fractal feature enhancement." Expert Systems with Applications **39**(3): 2804-2812.

Gulski, E. (1993). "Computer-aided measurement of partial discharges in HV equipment." IEEE Transactions on Electrical Insulation **28**(6): 969-983.

Gulski, E., et al. (2002). "Knowledge rules support for CBM of power cable circuits." Cigre Paris.

Hao, L. and P. L. Lewin (2010). "Partial discharge source discrimination using a support vector machine." IEEE Transactions on Dielectrics and Electrical Insulation **17**(1): 189-197.

Hao, L., et al. (2006). Comparison of support vector machine based partial discharge identification parameters. Conference Record of the 2006 IEEE International Symposium on Electrical Insulation.

Harbaji, M., et al. (2015). "Classification of common partial discharge types in oil-paper insulation system using acoustic signals." IEEE Transactions on Dielectrics and Electrical Insulation **22**(3): 1674-1683.

Hong, T., et al. (1996). "PD classification by a modular neural network based on task decomposition." IEEE Transactions on Dielectrics and Electrical Insulation **3**(2): 207-212.

Hoof, M., et al. (1997). "PD source identification with novel discharge parameters using counterpropagation neural networks." IEEE Transactions on Dielectrics and Electrical Insulation **4**(1): 17-32.

Hui, B., et al. (2016). The relationship between partial discharge behavior and the degradation of 10 kV XLPE cable joints. 2016 International Conference on Condition Monitoring and Diagnosis (CMD).

Hunter, J., et al. (2010). Comparison of two partial discharge classification methods. Electrical Insulation (ISEI), Conference Record of the 2010 IEEE International Symposium on, IEEE.

Hunter, J., et al. (2013). "Autonomous classification of PD sources within three-phase 11 kV PILC cables." IEEE Transactions on Dielectrics and Electrical Insulation **20**(6): 2117-2124.

Illias, H., et al. (2012). Partial discharge patterns in high voltage insulation. Power and Energy (PECon), 2012 IEEE International Conference on, IEEE.

Illias, H. A. (2011). Measurement and simulation of partial discharges within a spherical cavity in a solid dielectric material, University of Southampton.

Illias, H. A., et al. (2015). "Transformer incipient fault prediction using combined artificial neural network and various particle swarm optimisation techniques." PloS one **10**(6): e0129363.

James, R. and B. Phung (1995). "Development of computer-based measurements and their application to PD pattern analysis." IEEE Transactions on Dielectrics and Electrical Insulation **2**(5): 838-856.

Janus, P. (2012). Acoustic Emission Properties of Partial Discharges in the time-domain and their applications.

Jay, F. and J. Goetz (1988). IEEE standard dictionary of electrical and electronics terms, Institute of Electrical and Electronics Engineers.

Jin, J., et al. (2006). "Classification of partial discharge events in gas-insulated substations using wavelet packet transform and neural network approaches." IEE Proceedings-Science, Measurement and Technology **153**(2): 55-63.

Jing, C. and J. Hou (2015). "SVM and PCA based fault classification approaches for complicated industrial process." Neurocomputing **167**: 636-642.

Karmakar, S., et al. (2009). Partial discharge measurement of transformer with ICT facilities. Power Systems, 2009. ICPS'09. International Conference on, IEEE.

Karthikeyan, B., et al. (2008). "Partial discharge pattern classification using composite versions of probabilistic neural network inference engine." Expert Systems with Applications **34**(3): 1938-1947.

Karthikeyan, B., et al. (2005). "Conception of complex probabilistic neural network system for classification of partial discharge patterns using multifarious inputs." Expert Systems with Applications **29**(4): 953-963.

Khan, Y., et al. (2014). "Partial discharge pattern analysis using support vector machine to estimate size and position of metallic particle adhering to spacer in GIS." Electric Power Systems Research **116**: 391-398.

Kreuger, F. H., et al. (1993). "Classification of partial discharges." IEEE Transactions on Electrical Insulation **28**(6): 917-931.

Kuffel, J. and P. Kuffel (2000). High voltage engineering fundamentals, Elsevier.

Lai, K. X., et al. (2010). "Application of data mining on partial discharge part I: predictive modelling classification." IEEE Transactions on Dielectrics and Electrical Insulation **17**(3): 846-854.

Lalitha, E. M. and L. Satish (1998). "Fractal image compression for classification of PD sources." IEEE Transactions on Dielectrics and Electrical Insulation **5**(4): 550-557.

Lalitha, E. M. and L. Satish (2000). "Wavelet analysis for classification of multi-source PD patterns." IEEE Transactions on Dielectrics and Electrical Insulation **7**(1): 40-47.

Lei, Z., et al. (2014). "Partial discharges of cavities in ethylene propylene rubber insulation." IEEE Transactions on Dielectrics and Electrical Insulation **21**(4): 1647-1659.

Lek, S. and J.-F. Guégan (1999). "Artificial neural networks as a tool in ecological modelling, an introduction." Ecological modelling **120**(2-3): 65-73.

Lemke, E. (2013). "Analysis of the partial discharge charge transfer in extruded power cables." IEEE Electrical Insulation Magazine **29**(1): 24-28.

Li, J., et al. (2006). "Partial discharge image recognition using a new group of features." IEEE Transactions on Dielectrics and Electrical Insulation **13**(6).

Li, L., et al. (2015). "Partial discharge recognition in gas insulated switchgear based on multi-information fusion." IEEE Transactions on Dielectrics and Electrical Insulation **22**(2): 1080-1087.

Ling, Y., et al. (2018). SVM-based Partial Discharge Pattern Classification for GIS. Journal of Physics: Conference Series, IOP Publishing.

Lu, Y., et al. (2018). Partial Discharges Pattern Classification in High Voltage Circuit Breakers. IOP Conference Series: Earth and Environmental Science, IOP Publishing.

Ma, H., et al. (2013). "Pattern recognition techniques and their applications for automatic classification of artificial partial discharge sources." IEEE Transactions on Dielectrics and Electrical Insulation **20**(2): 468-478.

Ma, X., et al. (2002). "Interpretation of wavelet analysis and its application in partial discharge detection." IEEE Transactions on Dielectrics and Electrical Insulation **9**(3): 446-457.

Majidi, M., et al. (2015). "Partial discharge pattern recognition via sparse representation and ANN." IEEE Transactions on Dielectrics and Electrical Insulation **22**(2): 1061-1070.

Majidi, M. and M. Oskuoee (2015). "Improving pattern recognition accuracy of partial discharges by new data preprocessing methods." Electric Power Systems Research **119**: 100-110.

Mardiana, R. and C. Q. Su (2010). "Partial discharge location in power cables using a phase difference method." IEEE Transactions on Dielectrics and Electrical Insulation **17**(6): 1738-1746.

Mas'ud, A., et al. (2016). "Artificial neural network application for partial discharge recognition: Survey and future directions." Energies **9**(8): 574.

Mazroua, A. A., et al. (1995). "Neural network system using the multi-layer perceptron technique for the recognition of PD pulse shapes due to cavities and electrical trees." IEEE Transactions on Power Delivery **10**(1): 92-96.

Mazroua, A. A., et al. (1993). "PD pattern recognition with neural networks using the multilayer perceptron technique." IEEE Transactions on Electrical Insulation **28**(6): 1082-1089.

Meruelo, A. C., et al. (2016). "Improved system identification using artificial neural networks and analysis of individual differences in responses of an identified neuron." Neural Networks **75**: 56-65.

Metwally, I. (2004). "Status review on partial discharge measurement techniques in gas-insulated switchgear/lines." Electric Power Systems Research **69**(1): 25-36.

Michael, N. (2005). *Artificial intelligence a guide to intelligent systems*, Addison Wesley.

Mohamed, F. P., et al. (2013). "The use of power frequency current transformers as partial discharge sensors for underground cables." IEEE Transactions on Dielectrics and Electrical Insulation **20**(3): 814-824.

Mohamed, F. P., et al. (2014). "Remote monitoring of partial discharge data from insulated power cables." IET science, measurement & technology **8**(5): 319-326.

Montanari, G. C., et al. (2006). "A new approach to partial discharge testing of HV cable systems." IEEE Electrical Insulation Magazine **22**(1): 14-23.

Mota, H. d. O., et al. (2011). "Partial discharge signal denoising with spatially adaptive wavelet thresholding and support vector machines." Electric Power Systems Research **81**(2): 644-659.

Noske, S. and A. Rakowska (2014). Off-line partial discharge measurements as a new data source about the technical condition of MV cables. 2014 ICHVE International Conference on High Voltage Engineering and Application.

Press, W. H., et al. (1989). Numerical recipes in Pascal: the art of scientific computing, Cambridge University Press.

Pylarinos, D., et al. (2011). "Impact of noise related waveforms on long term field leakage current measurements." IEEE Transactions on Dielectrics and Electrical Insulation **18**(1).

Raymond, W. J. K. and H. A. Illias (2017). "Classification of partial discharge measured under different levels of noise contamination." PloS one **12**(1): e0170111.

Sabat, A. (2011). Simulation of partial discharge in high voltage power equipment.

Sahoo, N. C., et al. (2005). "Trends in partial discharge pattern classification: a survey." IEEE Transactions on Dielectrics and Electrical Insulation **12**(2): 248-264.

Salomon, D. (2004). Data compression: the complete reference, Springer Science & Business Media.

Satish, L. and W. S. Zaengl (1994). "Artificial neural networks for recognition of 3-d partial discharge patterns." IEEE Transactions on Dielectrics and Electrical Insulation **1**(2): 265-275.

Schwarz, R., et al. (2005). Partial discharge detection in oil with optical methods. Dielectric Liquids, 2005. ICDL 2005. 2005 IEEE International Conference on, IEEE.

Sharkawy, R. M., et al. (2007). "SVM classification of contaminating particles in liquid dielectrics using higher order statistics of electrical and acoustic PD measurements." IEEE Transactions on Dielectrics and Electrical Insulation **14**(3): 669-678.

Sheng, B., et al. (2014). "Partial discharge pulse propagation in power cable and partial discharge monitoring system." IEEE Transactions on Dielectrics and Electrical Insulation **21**(3): 948-956.

Shurrab, I., et al. (2013). "RF-based monitoring and classification of partial discharge on wet silicone rubber surface." IEEE Transactions on Dielectrics and Electrical Insulation **20**(6): 2188-2194.

Song, X., et al. (2007). "Second generation wavelet transform for data denoising in PD measurement." IEEE Transactions on Dielectrics and Electrical Insulation **14**(6).

Soong, T. T. (2004). Fundamentals of probability and statistics for engineers, John Wiley & Sons.

Standard, I. (2000). "High-voltage test techniques: partial discharge measurements." IEC-60270.

Stone, G. C. (2005). "Partial discharge diagnostics and electrical equipment insulation condition assessment." IEEE Transactions on Dielectrics and Electrical Insulation **12**(5): 891-904.

Su, C. Q. and C. R. Li (2013). "Using very-low-frequency and oscillating-wave tests to improve the reliability of distribution cables." IEEE Electrical Insulation Magazine **29**(1): 38-45.

Subasi, A. and M. Ismail Gursoy (2010). "EEG signal classification using PCA, ICA, LDA and support vector machines." Expert Systems with Applications **37**(12): 8659-8666.

Sukma, T. R., et al. (2018). Classification of Partial Discharge Sources using Waveform Parameters and Phase-Resolved Partial Discharge Pattern as Input for the Artificial Neural Network. 2018 Condition Monitoring and Diagnosis (CMD).

Suzuki, H. and T. Endoh (1992). "Pattern recognition of partial discharge in XLPE cables using a neural network." IEEE Transactions on Electrical Insulation **27**(3): 543-549.

Tao, H. and M. T. C. Fang (2001). "Detection and classification of partial discharge using a feature decomposition-based modular neural network." IEEE Transactions on Instrumentation and Measurement **50**(5): 1349-1354.

Tenbohlen, S., et al. (2008). "Partial discharge measurement in the ultra high frequency (UHF) range." IEEE Transactions on Dielectrics and Electrical Insulation **15**(6): 1544-1552.

Tian, Y., et al. (2002). "Comparison of on-line partial discharge detection methods for HV cable joints." IEEE Transactions on Dielectrics and Electrical Insulation **9**(4): 604-615.

Venkatesh, S. and S. Gopal (2011). "Orthogonal least square center selection technique – A robust scheme for multiple source Partial Discharge pattern recognition using Radial Basis Probabilistic Neural Network." Expert Systems with Applications **38**(7): 8978-8989.

Venkatesh, S. and S. Gopal (2011). "Robust Heteroscedastic Probabilistic Neural Network for multiple source partial discharge pattern recognition – Significance of outliers on classification capability." Expert Systems with Applications **38**(9): 11501-11514.

Yaacob, M., et al. (2014). "Review on partial discharge detection techniques related to high voltage power equipment using different sensors." Photonic sensors **4**(4): 325-337.

Zhang, H., et al. (2007). "A novel wavelet transform technique for on-line partial discharge measurements. 1. WT de-noising algorithm." IEEE Transactions on Dielectrics and Electrical Insulation **14**(1).

Zhang, X., et al. (2014). "GIS partial discharge pattern recognition based on the chaos theory." IEEE Transactions on Dielectrics and Electrical Insulation **21**(2): 783-790.